Chapter 4

Three-D Structural Analysis: Method and Examples of Application

1) Preparation of serial sections

Serial microscopic sections (Fig. 4-1)

The first step of 3-D structural analysis is to prepare serial sectional (2-D) images of material one intends to study. Various 2-D images are available. The most familiar in the domain of pathology is of course microscopic serial sections (Fig. 4-1), but organ slices for macroscopic observation or ultrathin sections for electron microscopy, if sequentially prepared, can also be used.

In preparing serial microscopic sections using a conventional type of microtome, I suggest to select carefully the embedding medium for the tissue to study. A material, if embedded in ordinary paraffin, may be prone to tearing and distortion at sectioning, which can create serious flaws in 3-D reconstruction. It seems that paraffin is not durable enough to allow us to make a set of flawless sections. To minimize the artifact, I advise to use celloidin-paraffin instead of ordinary paraffin as embedding medium. However there is a disadvantage inherent in this method: celloidin-paraffin sections do not promise good results when immunostained or silver impregnated. Also they are apt to wrinkle in the process of extension in a water bath.

Sometimes we need to study macroscopic or submacroscopic structures. In this case, microscopic sections from a tissue block, usually smaller than 3× 2 cm, cannot always cover the area of interest. The same difficulties will be encountered when spatial distribution of lesions in a large organ has to be studied. In such cases, preparation of serial organ slices is indispensable. If either the whole, or a part, of a fixed organ is to be sectioned, a practicable method is to "embed" the material in gelatin and slice a gelatin block with a ham slicer (Suzuki *et al*., 1988). This allows us to obtain good serial slices with suitable thickness, usually 1 to 1.5 mm. An example will be shown in Fig. 4-42, a set of "macroserials" of liver lobe surgically removed for carcinoma. Gelatin embedding is particularly desirable when a flabby material is to be serially sectioned. This would be understandable if you imagine that a material prone to transformation, like human pancreas or breast, has to be serially sliced, constantly at a thickness of 1 mm. The embedding procedure is quite simple: only to keep the fixed material in a container filled with 20% gelatin solution and cool it in a refrigerator. Gelatin solution can be replaced with 4 to 5% agar solution or 8% celloidin solution (in ether alcohol).

Sometimes, while performing 3-D mapping of lesions in an organ sliced into 1

Fig. 4-1. Serial microscopic sections prepared to study the 3-D structure of gastric adenocarcinoma. Stained by Azan-Mallory method.

mm-thick "macroserials," we are required to confirm microscopically where the lesion in question exists and is extending. In this case, the slices have to be re-embedded in paraffin so as to obtain microscopic sections stained with some appropriate method. Here one had better devise a slice holder to prevent the slices from being bent through the process of dehydration and embedding. We use a thin box made of veneer sheets, with 1 mm interior thickness; the veneer sheets were made porous so as to permit free flow and diffusion of embedding medium.

2) Abstraction of 2-D images from serial sections

Structure of interest: profile abstraction using a projector (Figs. 4-2, 4-3, 4-4)

First of all, we have to prepare serial 2-D drawings or pictures from a set of serial sections. These should contain the profiles of structures that are extracted from the microscopic pictures and are to be reconstructed. Suppose that you are going to reconstruct peripheral airways and arteries of lung from a set of serial sections. Besides airways and arteries, microscopic pictures of lung contain "noises," the components that are not necessary and should be excluded: veins, connective tissue wrapping airways and blood vessels, interlobular and alveolar septa, and if there are inflammatory changes, exudates or granulation tissue. This is the very reality of microscopic pictures, and from these, one has to pick up only the profiles of airways and arteries. In most cases, recognition and extraction of necessary images have to be done with our

Fig. 4-2. A profile microprojector, Nikon model V-16C, useful for picking up necessary contours of structure from serial sections at various magnification.

own eyes and hands. As yet, we are not in the stage of technical development in which we can leave this laborious job to a computer-driven robot. An automatic extraction of profiles can be expected only when in a material, a certain microstructure is marked by fluorescent immunohistochemistry and submitted to image acquisition using a fluorescence microscope. A laser confocal microscope, if available, enables one to scan the tissue along the z-axis and obtain continuously changing, fluorescent sectional images (tissue tomograms) which can be conveyed to a computer for 3-D reconstruction in the display. However, this is essentially a sort of (transmission) light microscope, so that there is a limit in the tissue thickness (usually less than hundred μm), beyond which, opacity of tissue would make it hard to penetrate even for laser beam.

The best way to abstract the necessary images from serial microscopic sections, I think, is to use a profile projector of the type shown in Fig. 4-2. This is an optical device with which one can project a microscopic image on a screen at a magnification from ×5 to ×200. If a mercury bulb is available as the light source, one can obtain pictures of higher magnification, up to ×1,000. Usually, images are projected onto a

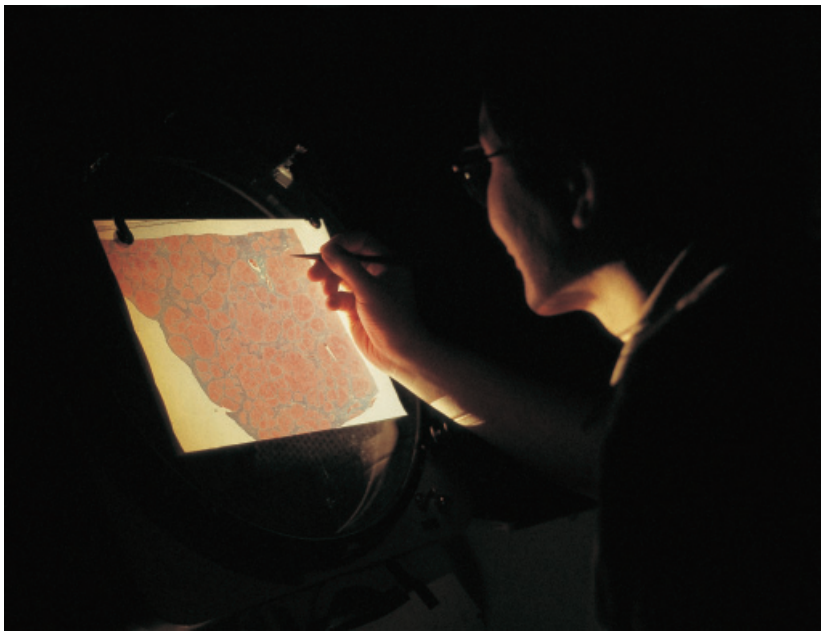

Fig. 4-3. Tracing of profiles to be reconstructed using the projector of Fig. 4-2. A sheet of tracing paper is placed on the screen, upon which the microscopic picture is projected at various magnification.

sheet of tracing paper placed on the screen, and the structures of interest are faithfully delineated along their profiles as in Fig. 4-3.

If a profile projector is not available, then try to project the optical field of microscope directly on a sheet of tracing paper using a simple, makeshift projector, an example of which is shown in Fig. 4-4. One only has to prepare a monocular microscope equipped with Köhler illumination. In a darkroom, a clearly focused projection of image is obtained at a distance 50 to 100 cm from the ocular lens. There is however a drawback in this method. The projected image is more or less distorted in the peripheral area of the round optical field due to spherical aberration inherent in the optical system, leaving only the central area adequate for analysis. Instead of delineating a projected image, you can of course use an enlarged microphotograph, but so long as relying on a microscope, aberration-free images are hard to obtain. In contrast, the profile projectors of the type shown in the foregoing figures are designed to keep the aberration below a minimum level so that they can serve specifically for the examination of precision products like semiconductors or microchips.

Sometimes, in performing reconstruction, accuracy is required to align sequential 2-D pictures rigorously with regard to the position and orientation. Several methods of alignment have been proposed. For example, one can rely on some guide marks such as the contour of the tissue block trimmed exactly vertically to the plane of section. Structures continuing in the tissue, such as the blood vessels, nerves etc., also serve as a guiding mark.

Fig. 4-4. A makeshift projector making use of a monocular microscope, equipped with Köhler illumination.

3) Manual reconstruction

Observation of 3-D by stacking serial images (Figs. 4-5, 4-6)

If a set of serial 2-D images have been completed, place the drawings sequentially on an X-ray film illuminator. Then the 3-D structure is visualized in a series of images gradually changing along the *z*-axis. In Fig. 4-5, serial pictures from an adenocarcinoma of stomach are stacked and looked through in order to see the 3-D form of cell nests. The result of observation can be expressed in the form of stereogram, *i.e.*, a manually drawn, graphic expression of spatial structure.

Figure 4-6 is another example of manual reconstruction aimed at visualizing the course and ending of the vasa efferentia of renal glomeruli (Takahashi, 1970). Normal renal cortex obtained at autopsy was serially sectioned, and reconstruction was per-

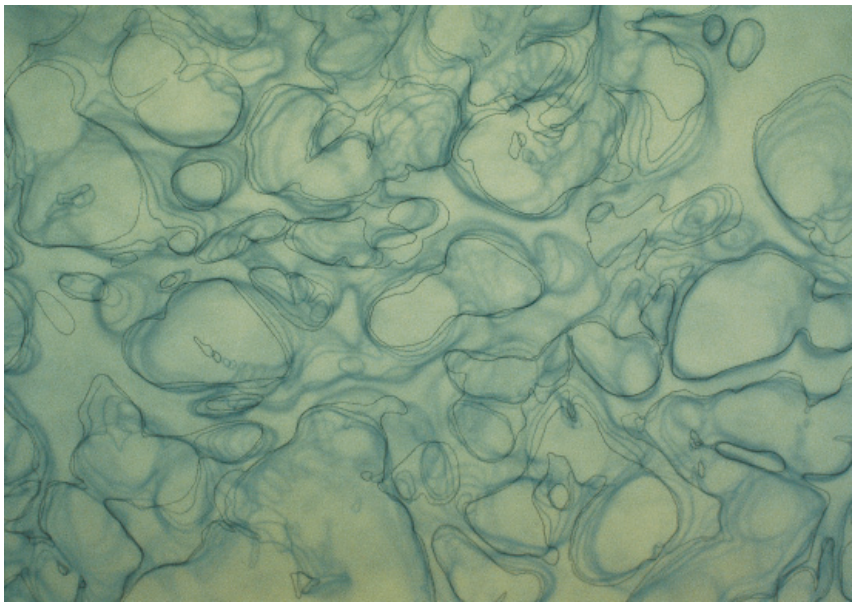

Fig. 4-5. A series of profile tracings are stacked and looked through upon an X-ray illuminator. From serial sections of moderately differentiated adenocarcinoma of the stomach. The 3-D structure of carcinomatous nests is clearly visualized.

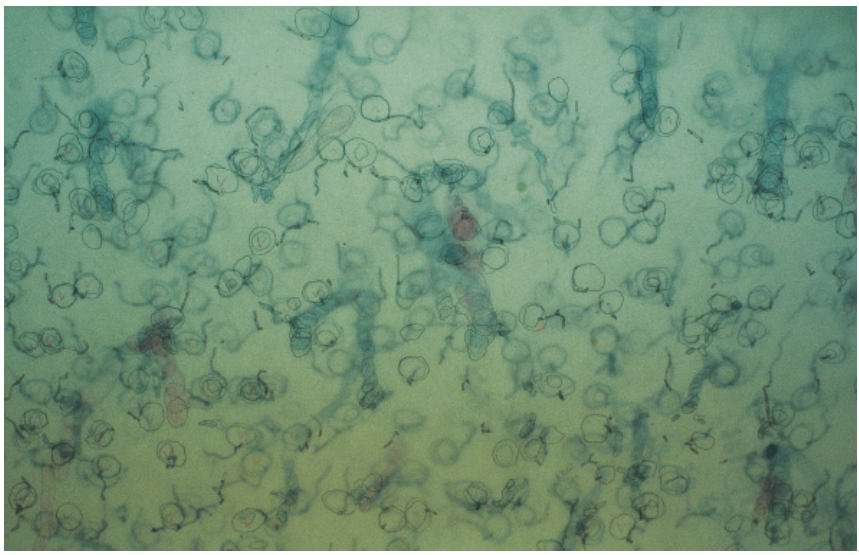

Fig. 4-6. A stack of serial tracings of normal kidney is looked through. The aim of this reconstruction was to see how vasa efferentia of glomeruli run in the cortical tissue and where they terminate. For this, hundreds of pairs of vasa efferentia and glomeruli were traced from serial sections of kidney.

formed over a thickness of 1.2 mm. All the glomeruli, vasa efferentia, veins and venules contained in the thickness were drawn. It was demonstrated that the vasa efferentia, 200 to 400 μm in length, have only sparse ramification, run through the cortical labyrinth and, interestingly, end at the outer boundary of the medullary ray without exception. The physiological significance of this distribution remains to be elucidated. In this example, the serial drawings were prepared at a thickness interval of 32 μm, i.e., every eight sections, with a single section 4 μm thick. Thus, there is no rule in the coarseness or fineness of reconstruction with regard to the inter-sectional interval, but from an economical and time-sparing viewpoint I would like to suggest to design a reconstruction study so that, the necessary knowledge may be obtained with a least number of serial images, if possible within 50 steps.

4) Computer-assisted reconstruction

Axial view of bronchus (Fig. 4-7)

Though simple and practicable with little expense, the manual method works only in studies dealing with an object which is relatively uncomplicated. If not, it sometimes happens that one is brought to confusion in a labyrinth of microstructure. When analyzing such a complicated structure as a 3-D network intertwined with blood vessels, one would be exhausted before completing a sufficiently accurate stereogram. Even if we manage to complete one, the stereogram only presents a picture viewed from a fixed angle, i.e., perpendicular to the plane of section. In reality, there are

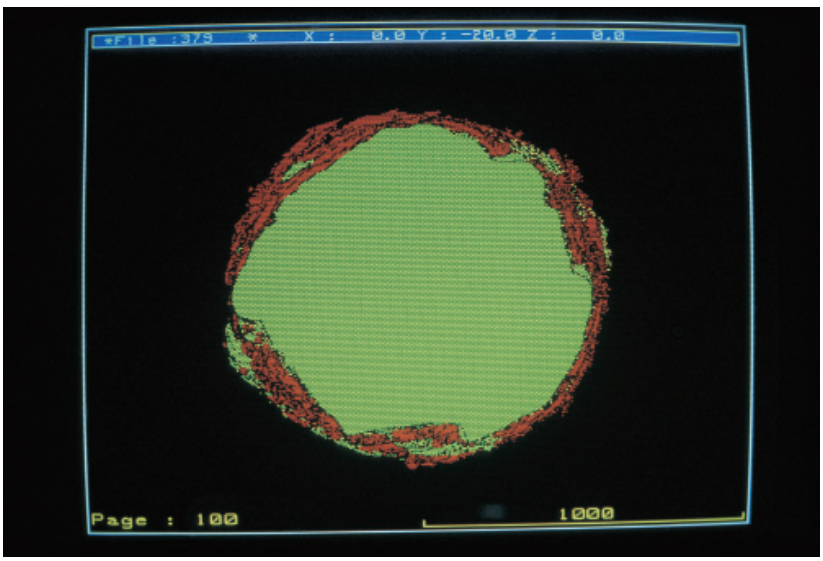

Fig. 4-7. Computer-aided reconstruction of a membranous bronchiole, presenting an axial view, in contrast to Fig. 1-11 where the same material is reproduced to show a lateral view. Reproduced from Yaegashi, Takahashi, *et al*. (1986): J Microsc 146, pp. 57.

instances in which we cannot attain a full understanding of 3-D structure unless views from different angles are combined. For example, figure 4-7 is a computer-assisted reconstruction of a bronchial segment which was serially cross sectioned. So long as relying on manual method, one would be unable to see, in its lateral view, how the smooth muscles (red) are arranged in the wall. This is however clearly visualized by resorting to a computer system which reproduces a lateral view of the segment as previously shown in Fig. 1-11. There the smooth muscles are shown following a spiral course with an inclination of about 25 degrees. This sort of image transformation cannot be attained without computer-assist.

A system assisting 3-D structural analysis (Fig. 4-8)

In 1986, our team designed a system for 3-D structural analysis for the study of pathology and microanatomy (Takahashi 1986; Yaegashi *et al.,* 1987), which was produced by what was a nascent team of engineers, that has since then developed into Rise Corporation, Sendai, Japan. Based on a desktop computer with a color display and a graphics tablet, this was probably the first reconstruction system designed for biomedical research and put to practical use (Fig. 4-8). The software, written in Hewlett-Packard BASIC at the first trial, has been updated several times, now working on WINDOWS. It covers basic functions of 3-D reconstruction including data input, data processing for visualization of 3-D structures at various magnification, style, color and angle, and basic 3-D measurement. A series of 2-D pictures are inputted from a graphics tablet where an image profile is digitized into a series of xy coordinate values. When a set of sequential 2-D pictures have been inputted, basic conditions for reconstruction are given, including the angle of viewpoint, the magnification of image, color for different structures or expression styles. Sometimes one need to repeat reconstruc-

Fig. 4-8. A system designed to assist the analysis of 3-D organ structure (OZ system, produced by Rise).

tion trial before obtaining an appropriate condition. Shown in the following are examples of reconstruction, some of which were performed by manual method before the advent of computer-assist.

5) Examples of 3-D reconstruction

a) The vasa vasorum of aortic wall

Vasa vasorum of the aorta (Fig. 4-9)

Larger arteries of adults like the aorta or pulmonary arteries are thick-walled, with the smooth muscle layer, called the media, as thick as 2.0 mm at the ascending aorta of a normal adult. In general, the smooth muscle cells of media is sustained in two ways. On one hand, the cells are considered to rely on oxygen and nutrients carried by molecular diffusion either from the luminal blood or from small vessels of the adventitia. The other media-sustaining mechanism is a continuous flow of plasmal fluid which is filtered through the endothelial barrier, permeates through the wall and drained by venules or lymphatics of the adventitia (Linzbach, 1958). However, it seems that when the medial thickness surpasses a certain limit, the artery can no longer sustain its medial layer without the aid of vasa vasorum. The vasa vasorum are minute blood vessels that penetrate the wall from the exterior of an artery. Distributed within the outer medial layer, they are considered to help the smooth muscle cells subsist. Figure 4-9 is a microphotograph of the outer medial layer and adventitia of normal human aorta. The adventitia is the layer of connective tissue one can find in the upper

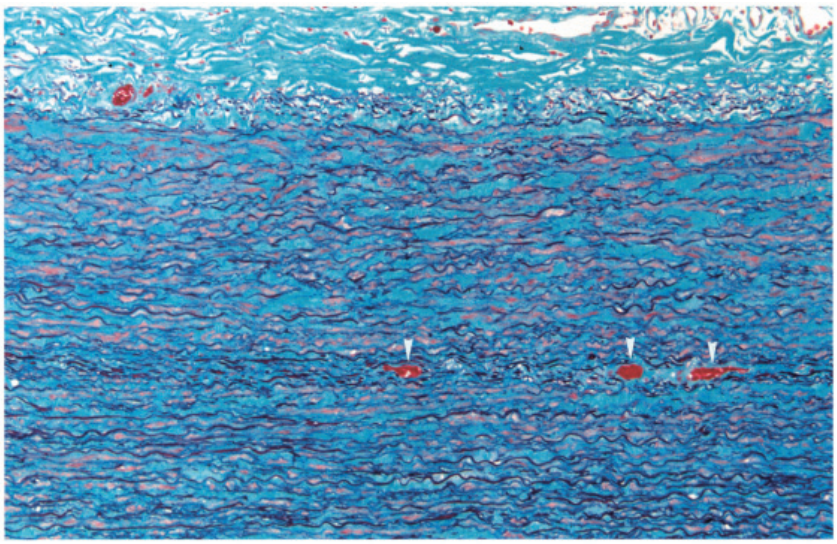

Fig. 4-9. Microscopic appearance of the human aortic wall to show the vasa vasorum (white arrowhead). The uppermost layer is the adventitia made of collagen (green). The vasa vasorum are minute vessels sporadically deployed in the outer layer of media. Elastica-Goldner stain.

1/4 of the figure where thick collagen fibers, stained in green, stack up. The lower 3/4 is the outer part of the media and here, a few vasa vasorum are deployed in the smooth muscle layer.

Density of vasa vasorum in the aortic wall: morphometry (Fig. 4-10)

Okuyama *et al*. (1988a) made a morphometric study of aorta and its large elastic type subbranches to make clear the relation between the thickness of arterial media and the development of vasa vasorum, with the latter expressed by the density of the tiny vessels in the medial layer. The left part of Fig. 4-10 illustrates the geometric significance of the density. In a cross-section of arterial wall, the number of vasa vasorum was counted along a sampling line (L), and the mean number N_L per a unit line length was calculated. N_L is a quantity proportionate to the mean total length L_A of vasa vasorum in a unit area A of wall (the length density in area). The result of measurement is shown in the right figure where the medial thickness D is shown in the abscissa, and L_A in the ordinate. The density of vasa vasorum rises as the arterial wall thickness D increases, and there is an intimate exponential correlation between L_A and D. Here one can see that the regression curve crosses the abscissa at $D = 0.6$, showing that in average, the vasa vasorum emerge when the medial thickness of an artery exceeds 0.6mm. In other words, the arterial media can be sustained in an avascular state only when it does not exceed this critical thickness.

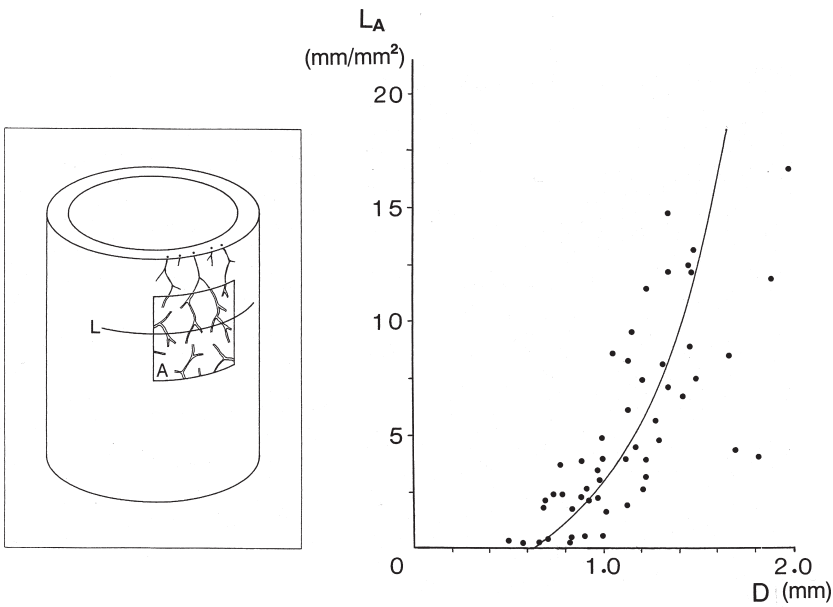

Fig. 4-10. The density of vasa vasorum in the aortic wall studied by morphometry. Left: the method of morphometry. Right: the density of vasa vasorum L_A plotted against the medial thickness D of the aortic wall. The density L_A is defined as the length density of the vessel per a unit area of aortic wall, as in the left. Note that the vasa vasorum develop exponentially along with the thickening of wall. Reproduced from Okuyama, Takahashi, *et al*. (1988): Arch Pathol Lab Med 112, pp. 723.

However, at the time the study of Okuyama *et al*. was performed, no information was available about the distribution of these minute vessels in the arterial wall, motivating the authors to undertake 3-D visualization (1988b).

Three-D structure: vasa vasorum of normal aorta (Figs. 4-11, 4-12)

Figure 4-11 is a schema illustrating how serial sections were prepared from arterial wall. A patch of wall tissue, about 1 × 1 cm, was taken from the wall of normal ascending aorta as in the figure. The material embedded flat in celloidin-paraffin was subjected to serial sectioning so as to produce the sections parallel to the wall surface.

The result of 3-D reconstruction is shown in Fig. 4-12 and presents what the vasa vasorum look like when observed from an angle vertical to the plane of aortic wall. The picture discloses quite a peculiar character of these vessels that perhaps one would be unable to find in any other part of the human body. First, it is shown that the media of the aorta is not provided with the usual network of capillaries. Instead, the vasa vasorum, while including terminal arterioles (shown red), venules (blue) and capillaries (beige), are distributed at a density that is strikingly low. They have been found to run in special tunnels that are penetrating the media as sparsely deployed tracts, with a pair of neighboring tunnels having a distance as large as 0.5 to 1.0 mm interposed between them, while in ordinary capillaries the mesh size does not exceed 0.15 mm. On account of this, we introduced a term "vascular cord" for these tracts. Second, it is clearly visualized that the vasa vasorum divide in the form of tree instead of network found in ordinary capillaries, and moreover, run in the tunnels as parallel double track. An inlet part of capillary forwards to and reaches the blind-ended terminal of tunnel,

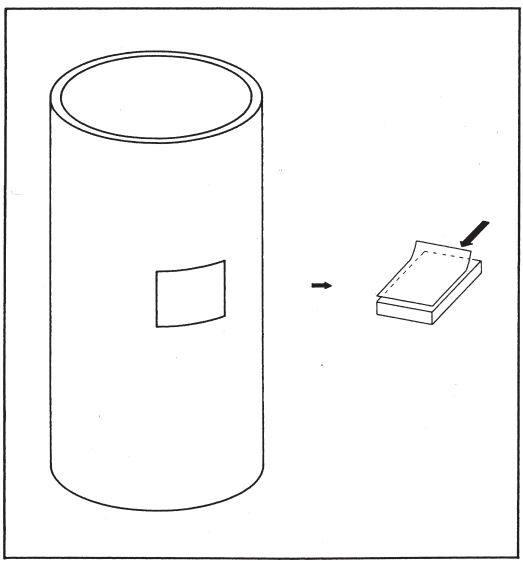

Fig. 4-11. A schema showing how and in what direction serial sections were prepared from the aortic wall. Reproduced from Okuyama, Takahashi, *et al.* (1988): Arch Pathol Lab Med 112, pp. 727.

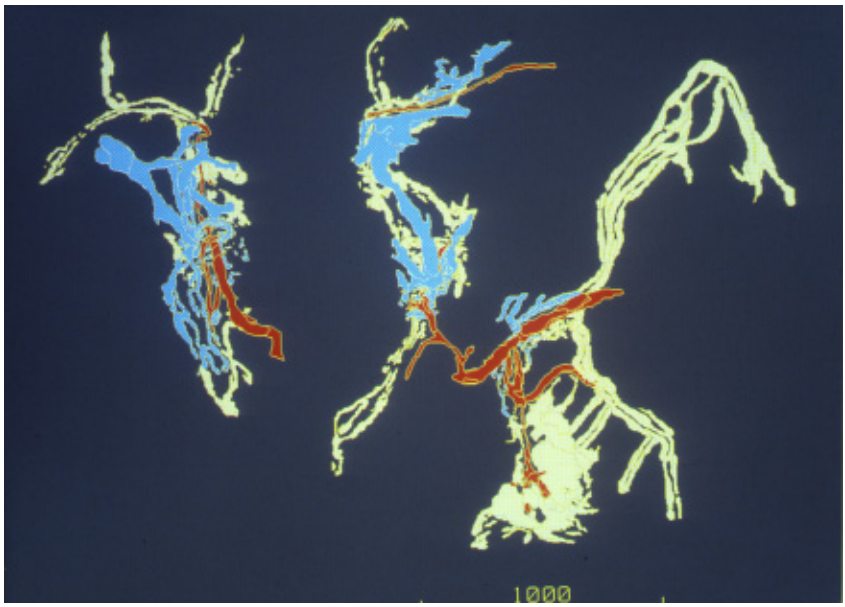

Fig. 4-12. Computer-assisted 3-D reconstruction of vasa vasorum in the wall (media) of normal aorta. A view vertical to the aortic wall from the outside. Painted red are inlet arterioles, blue are venules, and beige are capillaries. Reproduced from Okuyama, Takahashi, *et al*. (1988): Arch Pathol Lab Med 112, pp. 728.

where it takes a sharp U-turn and returns the way it had come. What is found here may be regarded as an extremely contiguous pattern of microvasculature (see Chapter 3), but we still have no idea on what type of microcirculation dominates in and around the vasa vasorum, or how the smooth muscle cells of media are assisted by these vessels.

b) Three-D mapping of vascular lesions in lungs with pulmonary hypertension

Pulmonary veno-occlusive disease: vascular changes (Figs. 4-13, 4-14)

Pulmonary veno-occlusive disease (PVOD) is a rare disorder of lung vessels, classified as a special type of primary pulmonary hypertension. Its etiology remains unknown. Figure 4-13 demonstrates the lung of a patient who had this disease and died of severe right-sided heart failure. One can find in the microphotograph two peripharal branches of pulmonary vein, both severely obstructed. In the alveolar tissue in the surroundings, there is extensive edema resulting from elevated pressure of capillaries in the alveolar septa due to impaired draining of blood.

An affected pulmonary vein is shown in Fig. 4-14. One can see the lumen is severely obstructed with fibrous tissue probably resulting from organized thrombus. However, in a 2-D section of lung, such obstructed veins are found only sporadically, so that one cannot evaluate how far the total vascular bed of lung is obstructed, without observing the distribution of lesion in the three dimensions.

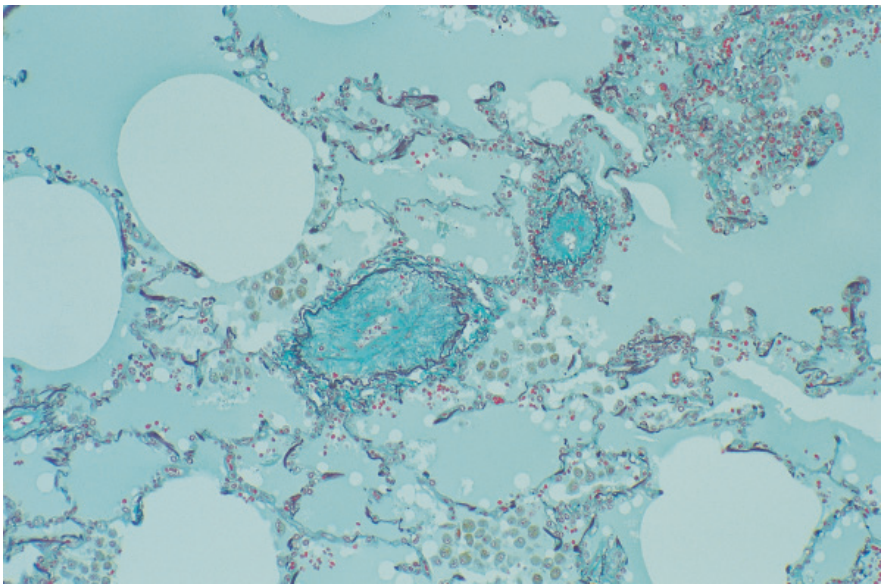

Fig. 4-13. A low power microphotograph of the lung of patient who died of cardiac (right ventricular) failure due to pulmonary veno-occlusive disease (PVOD). There are two small pulmonary veins, both severely obstructed. Extensive edema is visible in the alveolar tissue around the veins. Elastica-Goldner stain.

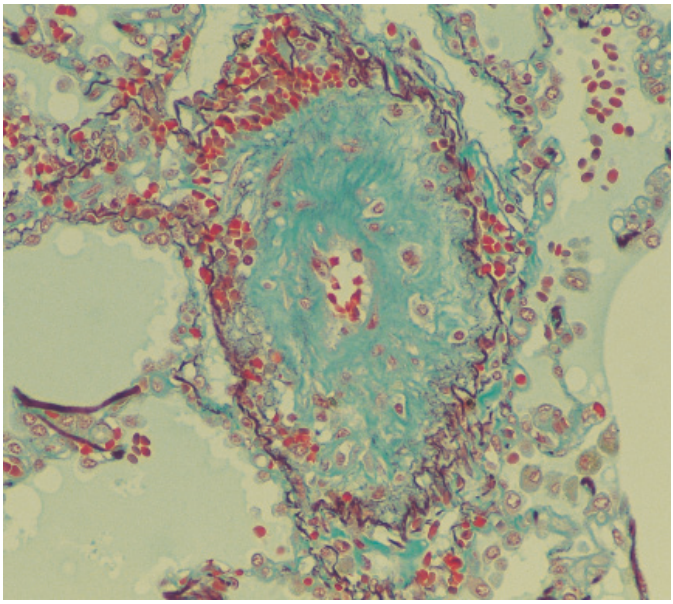

Fig. 4-14. A high power view of obstructed pulmonary vein. The lumen is obstructed with fibrous tissue resulting from organized thrombus. Elastica-Goldner stain.

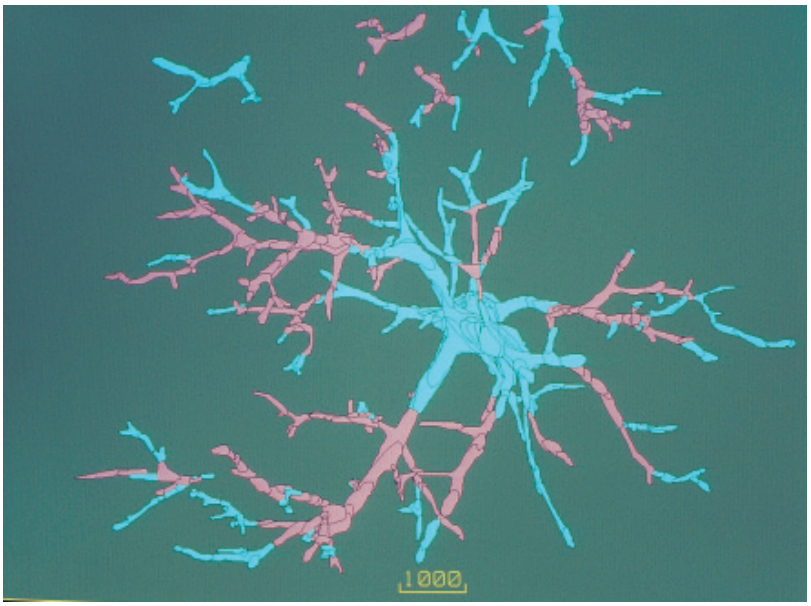

Fig. 4-15. Computer-aided 3-D reconstruction of pulmonary veins in the lung of PVOD patient shown in the previous figures. Obstructed segments are paited pink, non-obstructed segments light blue. The pulmonary venous bed is severely narrowed with few if any routes of drainage from the alveolar tissue toward the larger pulmonary veins.

Three-D mapping of obstruction in the pulmonary venous bed (Fig. 4-15)

Figure 4-15 is the result of computer-aided 3-D mapping where obstructed segments are shown in pink and those non-obstructed in light blue. The picture, while containing only peripheral venous trees with the largest segment having a diameter of about 350 μm, clearly demonstrates that obstructions are distributed in much smaller segments. One can trace routes of venous drainage from the treetops, and it may be clear that there remain few if any routes that are kept open. Thus, already the whole vascular bed has severely been stenosed, which however is apt to be underestimated on a single microscopic section.

Hypertensive pulmonary arteriopathy, Grade 1 (Fig. 4-16)

It is well known that some patients having congenital cardiac anomaly such as ventricular septal defect (VSD) are complicated by pulmonary hypertension (PH) which may be progressive, often bringing a fatal outcome. This is because if PH is sustained for a long time, obstructive lesions of small pulmonary arteries develop, gradually narrowing the vascular bed of lung in an irreversible way. The progression of this "hypertensive pulmonary arteriopathy" has been graded by the famous Heath-Edwards criteria (1958). In patients in whom arteriopathy has advanced too far, surgical correction of cardiac anomaly, for example closure of ventricular septal defect, has been considered equivalent to "opening the door of death," because it results in squeezing

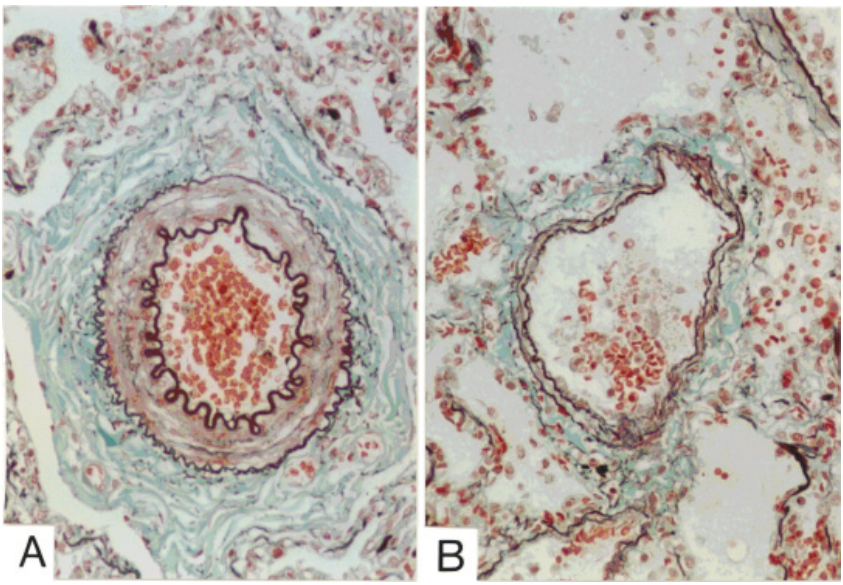

Fig. 4-16. Pulmonary artery with hypertensive pulmonary arteriopathy, Grade 1 (A), found in a patient of ventricular septal defect (VSD). The medial layer is strongly thickened as contrasted with an artery of about the same size, taken from a non-hypertensive (B). Elastica-Goldner stain.

an acutely increased blood volume into the already narrowed vascular bed. However, understanding has been and is still imperfect about to what degree the peripheral vascular bed of lung is obstructed by what type of lesion in what stage of hypertension. In view of this, Yaginuma *et al*. (1990) performed 3-D mapping of pulmonary arterial changes in surgical biopsy specimens of lung taken from several patients with congenital heart disease. Figure 4-16 left demonstrates the earliest change of pulmonary artery (Grade 1) where one can find only medial thickening due to hypertrophy of smooth muscles. This is from a patient of VSD, in whom the mean pulmonary arterial pressure was strongly elevated, reaching a level almost equal to the systemic blood pressure. Figure 4-16 right is a normal pulmonary artery of equivalent dimension. Note that the medial layer is markedly thinner.

Hypertensive pulmonary arteriopathy: Grade 2 and 3 (Figs. 4-17, 4-18)

Defined as Grade 2 are the arterial changes with the intima thickened due to proliferation of myointimal cells as in Fig. 4-17. Though moderately stenosing the lumen, this sort of change is considered to be reversible.

In the artery shown in Fig. 4-18, the intimal layer seems moderately thickened and consists of concentrically arranged deposit of hardened collagen. This lesion is defined as Grade 3 and for this, Wagenvoort and Wagenvoort (1977) coined an expression, the concentric laminar intimal fibrosis. The change has generally been considered to be a sign that the vascular disease has attained at an irreversible stage.

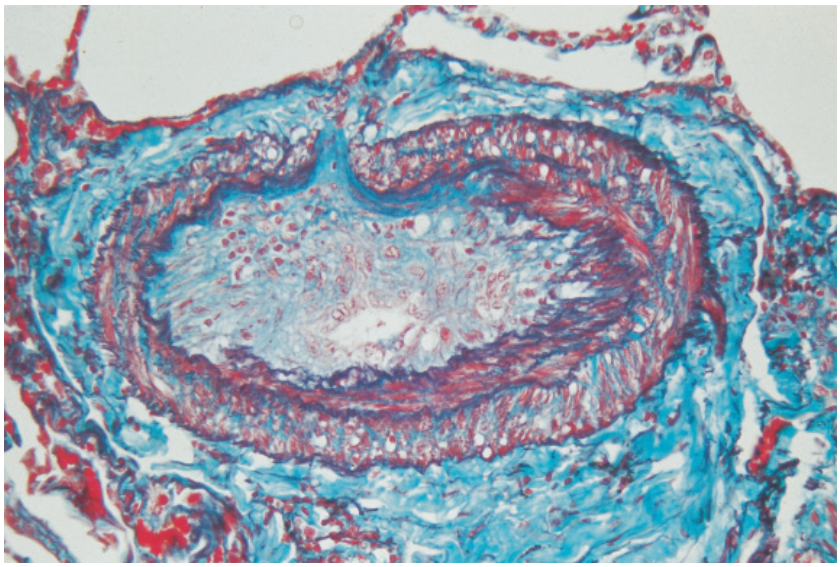

Fig. 4-17. Hypertensive pulmonary arteriopathy, Grade 2, with luminal stenosis brought about by cellular intimal proliferation. Elastica-Goldner stain.

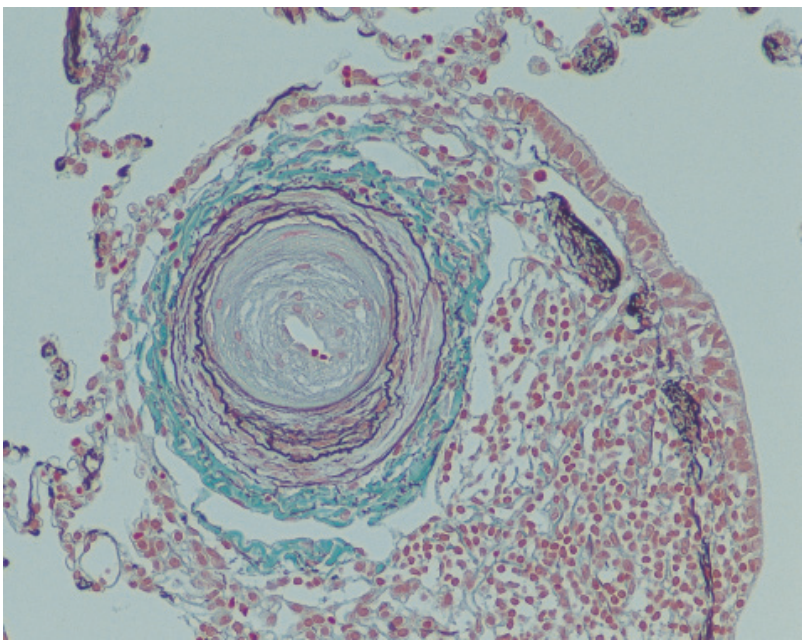

Fig. 4-18. Hypertensive pulmonary arteriopathy, Grade 3, a unique lesion called concentric laminar intimal fibrosis. Development of this lesion is considered to mark the watershed for the patients of pulmonary hypertension in whom surgical correction of cardiac anomaly is contraindicated. Elastica-Goldner stain.

Grade 4 and 5: plexiform lesion (Figs. 4-19, 4-20)

The severest form of arteriopathy is a unique change, generally called the plexiform lesion. Two examples of plexiform lesion are exhibited in Fig. 4-19. It involves a small pulmonary artery ranging from 100 to 150 μm in diameter and develops at a place shortly after the segment is divided off its parent artery (denoted by 1). The lesion presents as what may be expressed as a microaneurysm filled with fibrous tissue (2) that apparently is left after a massive thrombus has been organized. The term "plexiform" originates from the finding that the fibrous part of the lesion contains a network of small vessels. Around the lesion, one can find several ectatic vessels (3) which seem to function as collaterals bypassing the plexiform lesion. (We call these vessels the dilatation lesions although, in the original article by Heath and Edwards,

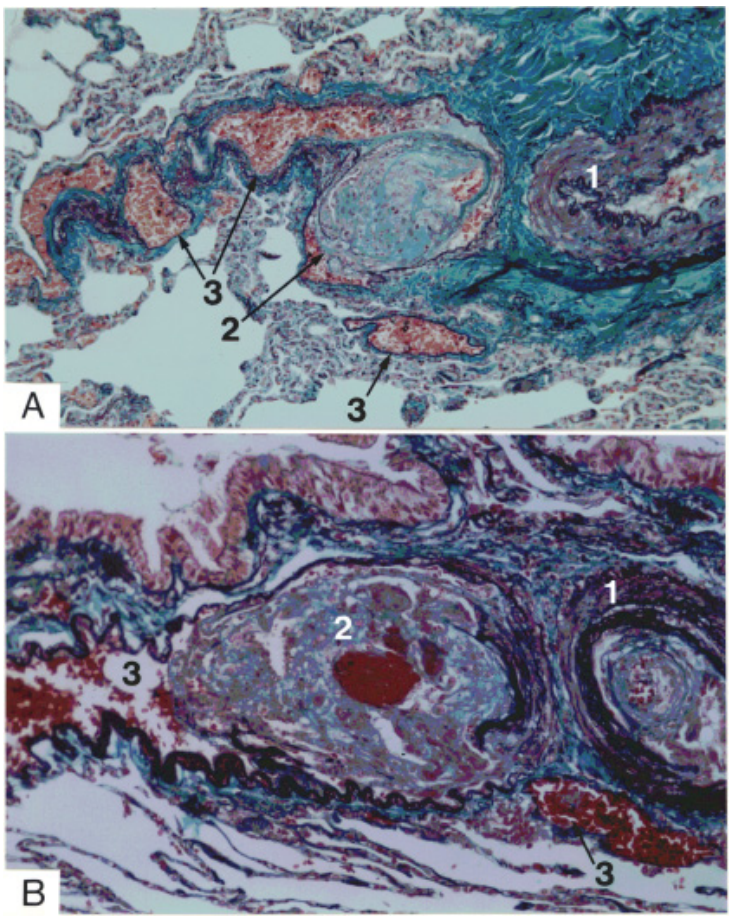

Fig. 4-19. Two examples of "plexiform lesion" defined as hypertensive pulmonary arteriopathy, Grade 4 to 5. The lesion develops in a small artery of 100 to 150 μm in diameter at a place shortly after its division off its parent artery (1). The lesion presents as a complex, with a sort of microaneurysm filled with fibrous mass penetrated by plexus-like small vessels (2), and several ectatic vessels (3) that bypass the microaneurysm. Elastica-Goldner stain.

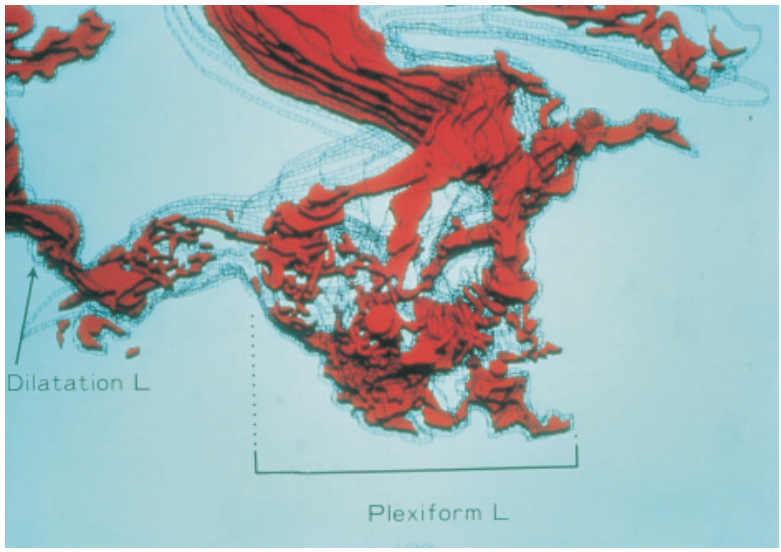

Fig. 4-20. Computer-aided 3-D reconstruction of the microaneurysmal portion of plexiform lesion, revealing plexus-like small vessels penetrating the fibrous mass filling the lumen. Reproduced from Yaginuma, Takahashi, *et al*. (1990): Thorax 45, pp. 589.

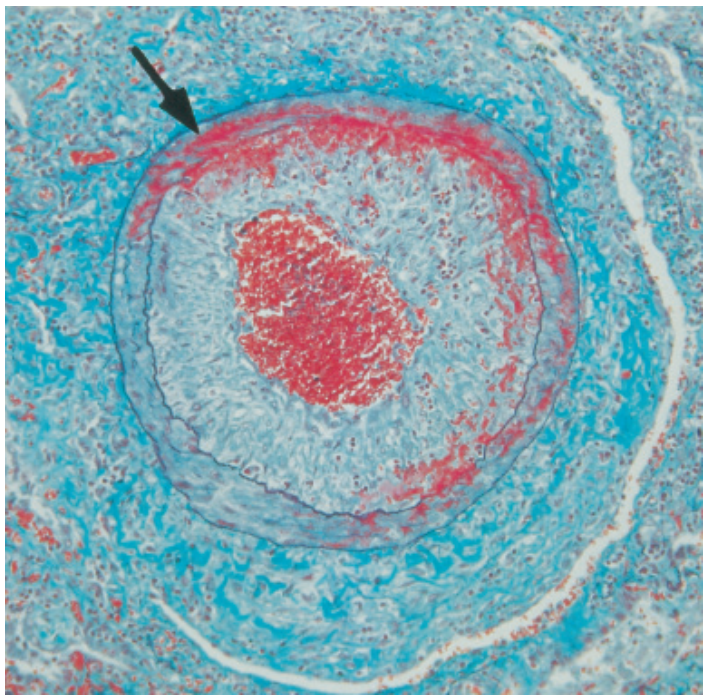

Fig. 4-21. Hypertensive pulmonary arteriopathy, Grade 6, that is marked by the development of pulmonary arteriitis. There is necrosis of medial smooth muscles infiltrated with fibrinoid material (arrow). Elastica-Goldner stain.

this term was given a wider connotation, including also the plexiform lesion) Usually, the presence of plexiform lesion is interpreted to be suggesting that in the patient, the disease is too far advanced to allow a radical cardiac surgery. It is said that a correction operation, if performed, can lead to a fatal outcome by acutely elevating the pulmonary arterial pressure that results in right-sided heart failure.

A plexiform lesion, when reconstructed, reveals that the inner mass of fibrous tissue is penetrated by a network of minute vascular channels, as in Fig. 4-20. It seems however that only less than 10% of normal blood flow is allowed to pass through the lesion.

Grade 6 lesion: arteriitis (Fig. 4-21)

In a terminal stage of PH, vasculitis of small pulmonary artery can develop and is designated as Grade 6 lesion. Figure 4-21 presents pulmonary arteriitis found in a patient of PH. The arrow denotes deposition of fibrinoid material (red). But this is only rarely encountered.

Three-D mapping of Grade 2 and 3 lesions (Fig. 4-22)

Figure 4-22 exhibits the result of 3-D mapping in a patient of VSD. Here the pulmonary arteries are shown to harbor Grade 2 (green) and Grade 3 (yellow) lesions, making the disease seem in a moderately advanced stage. One may recognize several

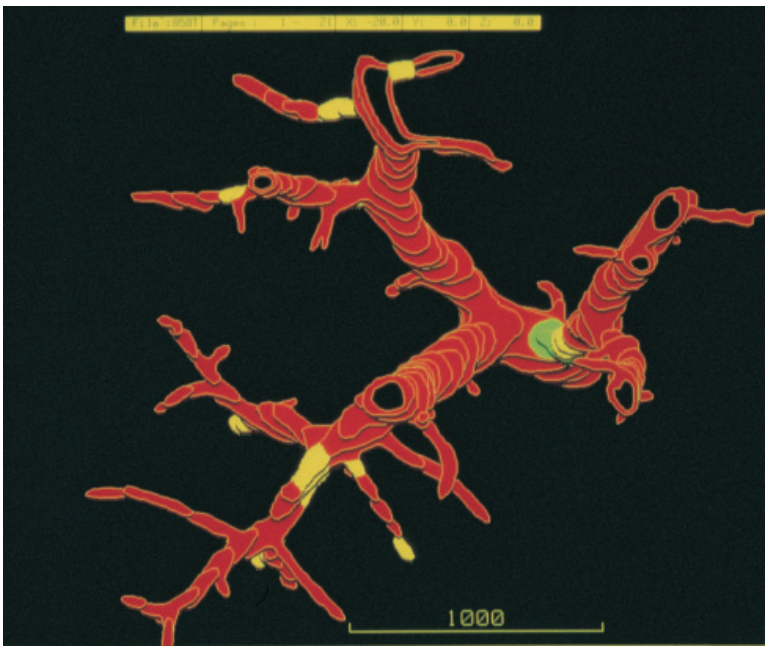

Fig. 4-22. Computer-assisted 3-D mapping of hypertensive arteriopathy in small pulmonary arteries. Moderately advanced case, with Grade 2 (green) and 3 (yellow) lesions. Note that as yet, more than half of the pathways are left open, allowing free flow to the alveolar area. Reproduced from Yaginuma, Takahashi, *et al*. (1990): Thorax 45, pp. 587.

flow routes that remain patent, where sufficient amount of blood can be led into the capillary region (the void space) without being blocked by obstructive changes.

Three-D mapping in advanced cases (Figs. 4-23, 4-24)

Figure 4-23 is from a more advanced case of VSD and demonstrates that many if not all arteries of about 150 μm in outer diameter are involved in either Grade 3 (light green) or Grade 4 (white) lesions. Still, there are small number of arterial flow routes remaining patent. Besides, it is clearly shown that the plexiform lesions involve only a specific site of pulmonary arterial tree, namely, "supernumerary" arteries of 150 μm in diameter arising from disproportionately large parent vessels. Anatomically, pulmonary arteries of this dimension correspond to those running in parallel with a respiratory bronchiole, i.e., those found in a 2-D section of lung at the entrance of pulmonary acinus.

Even in patients having plexiform lesions, the degree of arterial bed obstruction seems to be varying. Figure 4-24 is from another patient having plexiform lesions, but here one can no longer find any flow route that leads blood to the periphery. In other words, the arterial bed seems to be obstructed by 100%. In this patient, a certain, but not sufficient amount of pulmonary blood flow seems barely maintained through collateral pathways. Thus, even among advanced cases, difference seems to exist in the

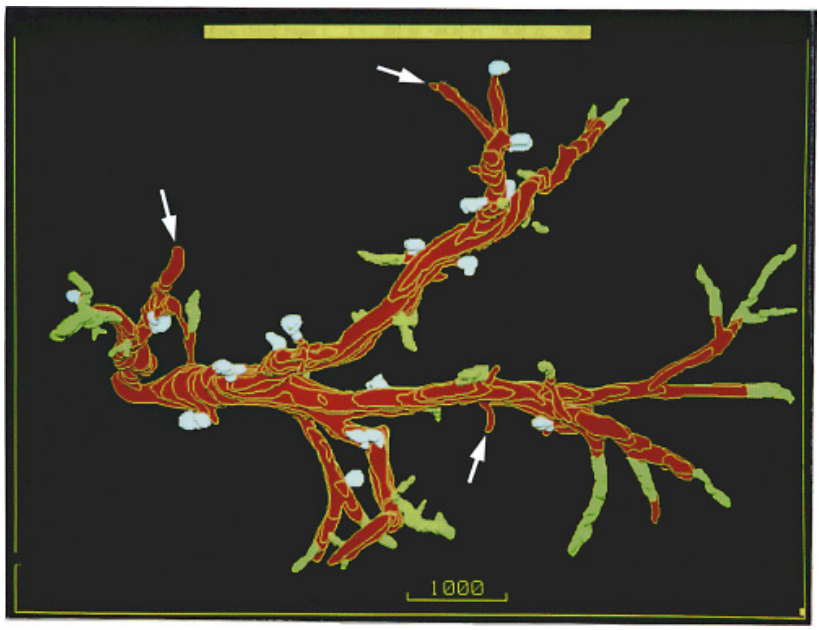

Fig. 4-23. Computer-assisted 3-D mapping of hypertensive arteriopathy in an advanced case. There are a number of plexiform lesions (white) and Grade 3 lesions (green), both involving a small pulmonary artery of 100 to 150 μm (the acinar arteries) shortly after their division from the parent artery. However the obstruction of vascular bed is not complete, with flow routes to the periphery remaining open at several places. Reproduced from Yaginuma, Takahashi, *et al*. (1990): Thorax 45, pp. 587.

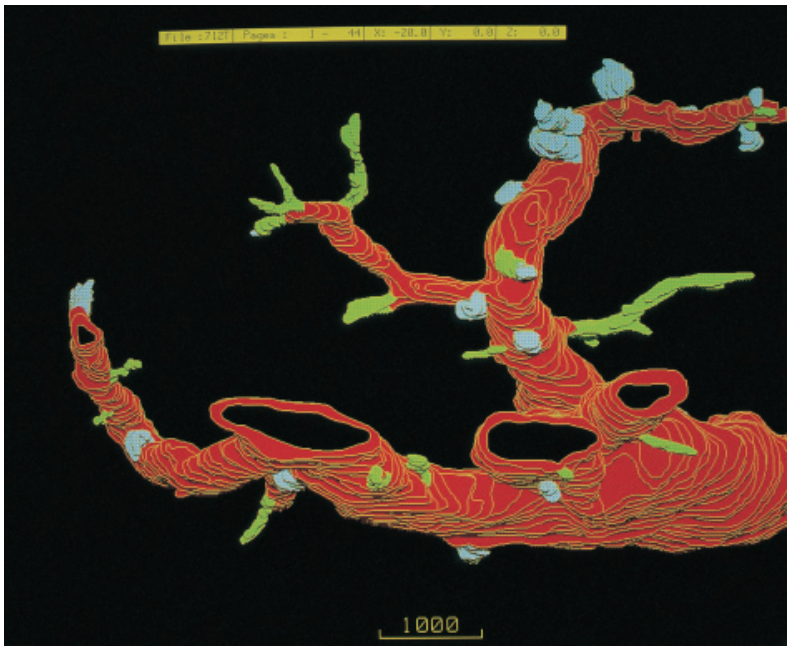

Fig. 4-24. Computer-assisted 3-D mapping of hypertensive arteriopathy in another advanced case. Here the flow routes to the periphery are entirely closed with plexiform (white) or Grade 3 (green) lesions.

degree to which the arterial bed is narrowed, and this makes us wonder whether a cardiac correction surgery should always and rigidly be contraindicated even when only a small number of Grade 4 lesions were detected on lung biopsy.

Studies were extended along this line by Matsuki *et al*. (1994). They attempted to estimate the grade to which the pulmonary vascular bed is narrowed in patients with congenital cardiac disease and pulmonary hypertension, by enumerating the Grade 3 and 4 lesions in a volume of lung. Sampling was done on serial sections and the numerical density of lesions N_V was calculated. The material included 17 autopsy lung specimens from different lobes of five patients dying of cardiac anomalies. All had advanced arteriopathies of pulmonary arteries. While performing computer-aided reconstrubtion, the number of lesions was enumerated on display. However, there was a problem: autopsy lungs are usually fixed in variously collapsed or overinflated state. With regard to this, standardization of lung volume was performed according to the method of Takahashi *et al*. (1983) who proposed to make use of the numerical density in lung section (N_A) of muscularized pulmonary arteries larger than 100 μm in external diameter, on the assumption that N_A may be constant, so long as the lungs are brought to a similar grade of inflation. The corrected N_V of vascular lesions thus obtained from patients with cardiac anomalies proved to be varying to an unexpected degree. Not only was there a marked difference between the individuals, but also among the site of lung within an individual. The degree of vascular bed narrowing, defined as the nu-

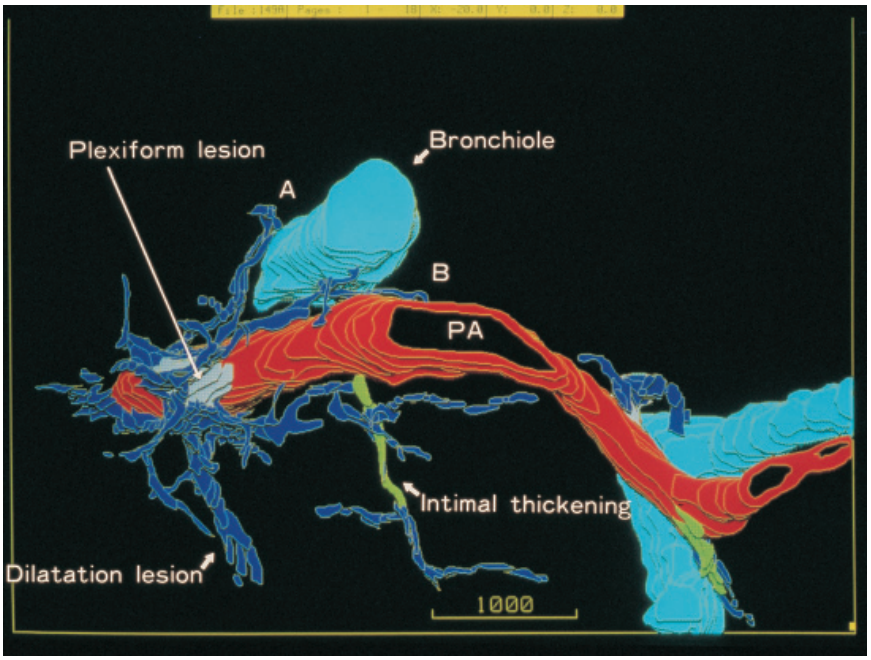

Fig. 4-25. Computer-assisted 3-D reconstruction performed to visualize the collateral pathways bypassing a plexiform lesion in an advanced case of pulmonary hypertension. A plexiform lesion (white) is bypassed by dilatation lesions (blue) developing in its surroundings. These varicose-vein-like ectatic vessels communicate on one hand with terminal bronchial arteries running along a bronchiole (A), and on the other, feed the wall of large pulmonary artery as its vasa vasorum (B). Thus, the dilatation lesions connect the bronchial and pulmonary arteries with peripheral capillaries. Reproduced from Yaginuma, Takahashi, *et al*.(1990): Thorax 45, pp. 588.

merical ratio of obstructed to the total of acinar arteries, was also various, suggesting that there can be operable patients who have a pulmonary vascular bed not so much narrowed even in the presence of Grade 4 lesions.

Plexiform lesion and its collaterals (Fig. 4-25)

Figure 4-25 is another reconstruction performed by Yaginuma *et al*. to visualize in an advanced case of pulmonary arteriopathy how collaterals develop and connect with what vessels. There is a plexiform lesion (white) developing in a small segment of pulmonary artery running along a respiratory bronchiole. Shown blue are "dilatation lesions" that in Fig. 4-19 presented as varicose-vein-like ectatic vessels meandering around the plexiform lesion and extending toward the alveolar capillaries. On the other hand, the dilatation lesions communicate with terminal bronchial arteries, either running along a bronchiole (A) or feeding the wall of pulmonary artery as its vasa vasorum (B). Thus, the dilatation lesions are so formed as to connect the bronchial arteries, pulmonary arteries and peripheral capillaries. This connecting relation suggests that the dilatation lesions are functioning as collaterals for the plexiform lesion.

c) Hypoplastic zone of myenteric plexus in Hirschspring's disease

The myenteric plexus and Hirschsprung's disease (Fig. 4-26)

The myenteric plexus (Auerbach's plexus) is autonomic nerve plexus of the intestinal wall, extending between the double-layered, longitudinal and circular, muscular coats. Normally it generates and controls the peristalsis of intestine by sending pulsatile stimuli.

One of the abnormalities involving the myenteric plexus is Hirschsprung's disease. This is a congenital disorder which brings about severe constipation of neonates emerging shortly after birth and lasting thereafter. The symptom has been attributed to lack of peristalsis in the distal part of the intestinal canal due to congenital agenesis of myenteric plexus in the wall of the paralytic segment (Whitehous, 1948). The extension of aganglionic zone, the zone where the plexus has not formed, varies from one patient to another; in some cases it involves only a short segment of the anal canal but in others, the paralytic zone can extend from the anal region to variable height, sometimes involving the whole large intestine and even the distal part of the small intestine. The sole treatment of this disease is surgical resection of the aganglionic segment. In order to determine the range of intestine to be resected, surgeons resort to intrasurgical biopsy of the bowel wall, taking a specimen from the height suspected to be slightly proximal to the border between the normal and aganglionic zones; if ganglion cells are confirmed to exist, the intestine below the height is removed. However, there is a problem: it has been assumed that the aganglionic zone does not begin abruptly but there is an "intermediate zone" between the normal and aganglionic zones: the inter-

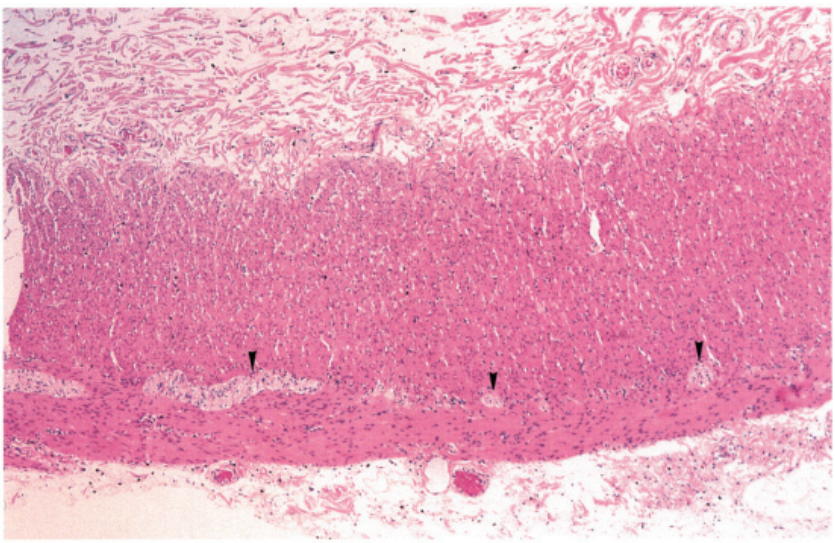

Fig. 4-26. Normal myenteric plexus. A microscopic picture of large intestine sectioned vertically to the wall. One can see sections of small ganglia and nerve bundles (arrowheads) deployed between the inner and outer layers of tunica muscularis propria. Hematoxylin-eosin stain.

mediate zone has seemed likely to be a segment of intestine where the plexus, though present, is so hypoplastic that when left unresected, the symptom may last after the operation. In fact, it has sometimes been experienced that various degree of constipation lingers even after surgery, and at least in a part of such cases, the transitional zone has been assumed to be remaining unremoved. Accordingly it seems desirable that, in performing an intrasurgical biopsy on frozen sections, the pathologist in charge could evaluate the grade of hypoplasia of the plexus. As yet, however, we are far from the state in which we can make a diagnosis of hypoplastic plexus with confidence, because the hypoplastic myenteric plexus has yet to be defined in clear morphological terms. To what degree does the thickness or density of nerve bundles are reduced in the hypoplastic zone? On what criteria can we rely in making diagnosis of hypoplasia when examining a 2-D section of bowel wall? Urged by these ambiguities, Miura *et al*. (1996) attempted to visualize the ordinary myenteric plexus and its changes in Hirschsprung's disease. No image of this sort has been presented so far. This will allow to compare the form of plexus between patients with Hirschsprung's disease and age-matched children on firm anatomical basis.

Figure 4-26 is a microphotograph showing the normal myenteric plexus in the wall of intestine. In a routine microscopic section which is cut vertical to the intestinal wall, the plexus appears as bundles of autonomic nerve, whose sections are scattered between the inner and outer muscular layers. Thus, to visualize the whole structure of the plexus, one needs to perform 3-D reconstruction so as to command the whole plexus in the form of network sandwiched between the two muscular layers.

Three-D structure of normal myenteric plexus (Fig. 4-27)

Figure 4-27 presents a 3-D reconstruction of myenteric plexus in the terminal part of normal ileum from a male infant aged 6 months. The serial sections were cut at a slight angle of 3 to 5 degrees with the plane of plexus. Only ganglia (nerve cell clusters) and nerve bundles that connect a pair of them were visualized. The plexus (green) is shown forming a network with the size of meshes somewhat uneven. The upper portion of the plexus corresponds to the proximal (oral) side of the intestinal patch, and the lower part, to the distal (anal) side. Note the thickness of individual nerve segments so as to compare with the next figure. An extrinsic nerve (blue) is shown joining the plexus.

The transitional and aganglionic zones in Hirschsprung's disease (Figs. 4-28, 4-29)

Figure 4-28 is a reconstruction of myenteric plexus in the transitional zone of intestine in Hirschsprung's disease. The patient was a male infant of 6 months, in whom the entire colon was involved in aganglionosis. Three-D reconstruction was performed at several places of intestine but the material for this figure was taken from the wall of the terminal ileum which is considered to be close to the transitional zone. Compared with the foregoing picture of normal control that was shown at the same magnification, the plexus is strikingly hypoplastic, with the individual bundles markedly thinner. Hypertrophic extrinsic nerves (blue) are also found joining the plexus.

Figure 4-29 is another reconstruction of the same bowel 1 cm distal to the area displayed in Fig. 4-28. Here one can see the last part of the transitional zone in the

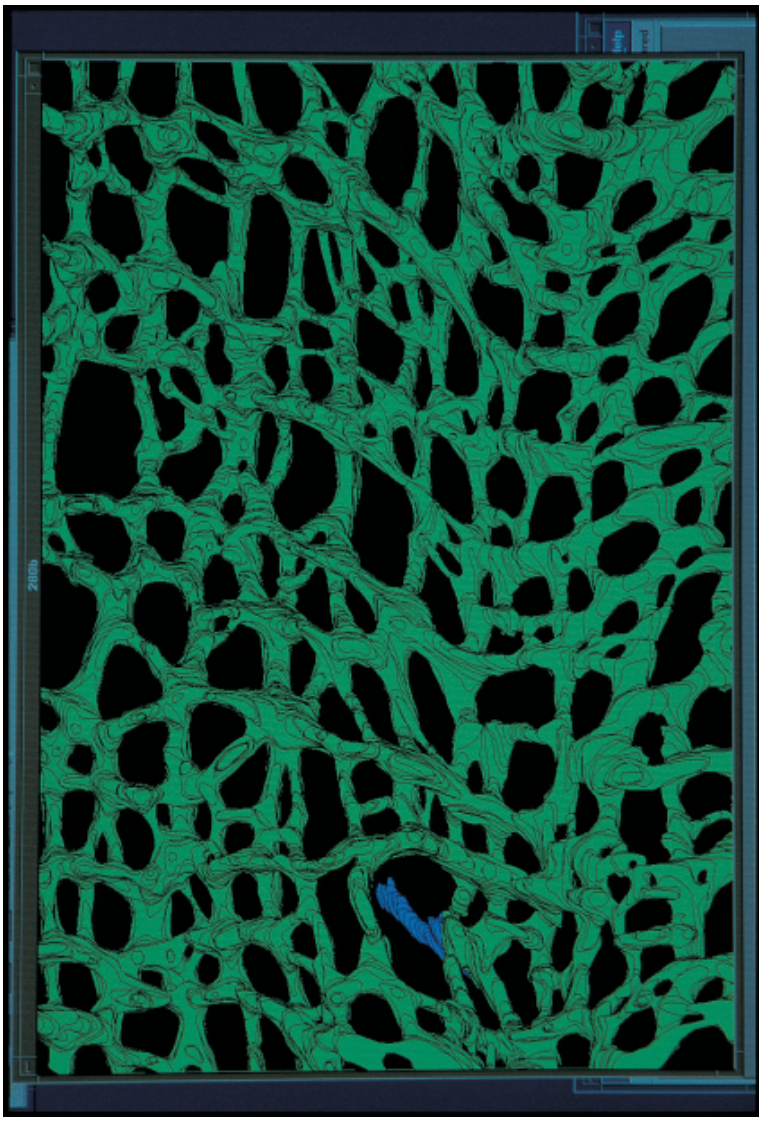

Fig. 4-27. Computer-assisted 3-D reconstruction of normal myenteric plexus, sandwiched between the inner and outer layers of tunica muscularis. Taken from the terminal part of ileum. The plexus presents as a dense, flat network where the connecting points of nerve bundles correspond to small ganglia. An extrinsic nerve (blue) joins the plexus. Reproduced from Miura, Takahashi, *et al*. (1996): J Pediat Surg 31, pp. 422.

upper, while at about the center of the figure, the aganglionic zone is beginning. In the latter zone extending toward the lower, one can find only small number of isolated ganglia.

Thus, the “transitional zone” of Hirschsprung's disease was clearly definable as an area extending over a certain length, where the density of network tapers toward the

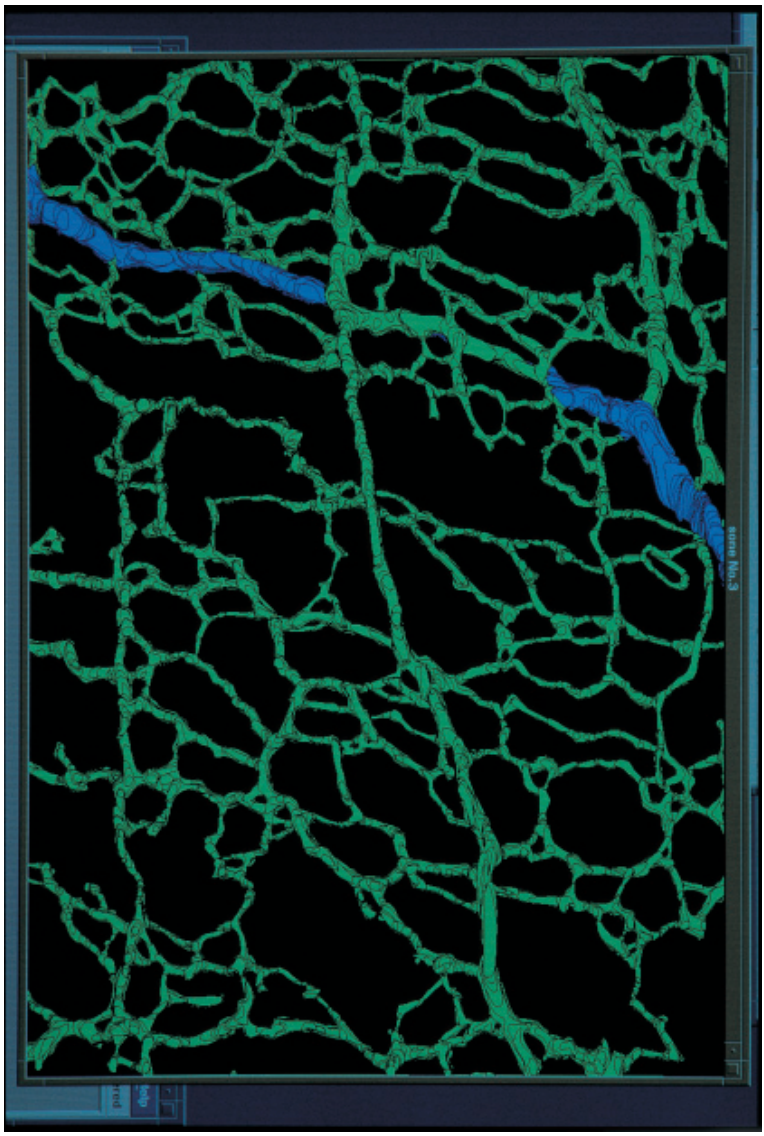

Fig. 4-28. Computer-assisted 3-D reconstruction of the transitional zone in the terminal ileum resected for Hirschsprung's disease, under the same magnification as in Fig. 4-27. Note the hypoplastic plexus, with the individual bundles markedly thinner as comparaed with the normal plexus. Reproduced from Miura, Takahashi, *et al*. (1996): J Pediat Surg 31, pp. 423.

aganglionic zone. This finding was considered to be of profound significance in designing a surgical strategy to prevent postoperative bowel dysfunction. A morphometric study was added to this by the same authors (Miura *et al*., 1995). They have con-

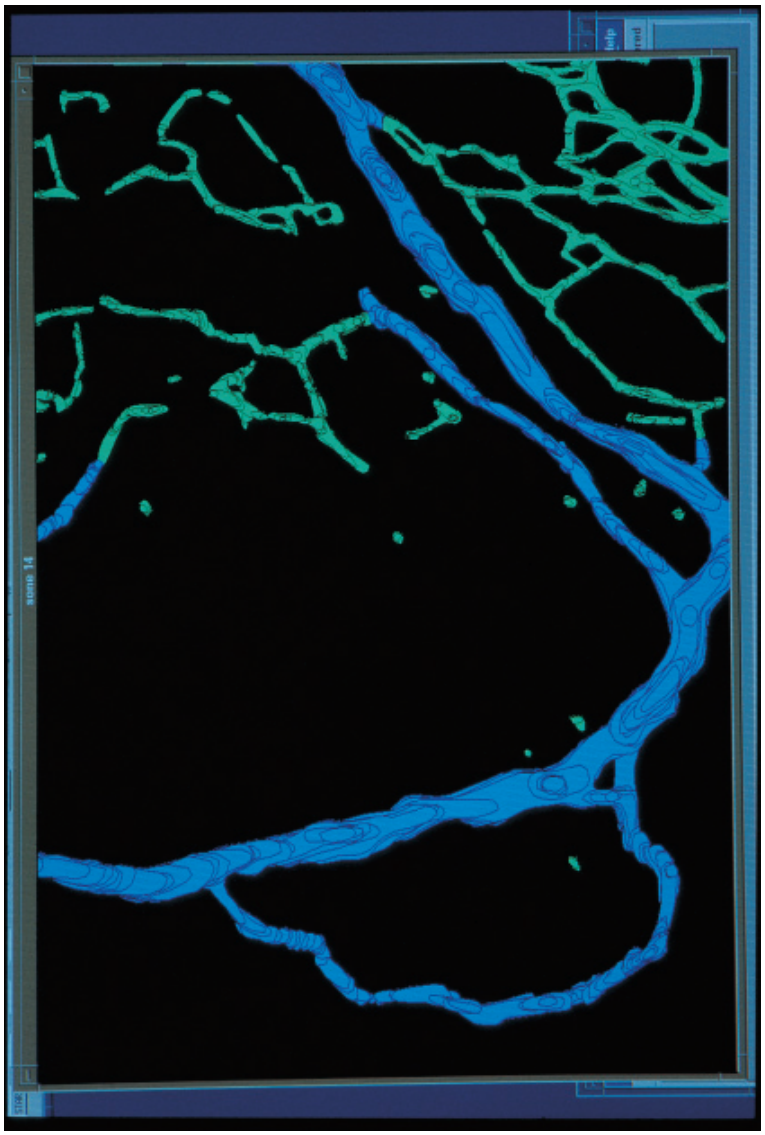

Fig. 4-29. Computer-assisted 3-D reconstruction of the myenteric plexus 1cm distal to the site reconstructed in Fig. 4-28. The terminal part of the transitional zone (upper) and the beginning part of the aganglionic zone (lower) are included. Reproduced from Miura, Takahashi, *et al*. (1996): J Pediat Surg 31, pp. 423.

firmed in intestines resected from four patients of Hirschsprung's disease that the extension of transitional zone in the longitudinal direction of intestine was various, ranging from 1cm to more than 5 cm.

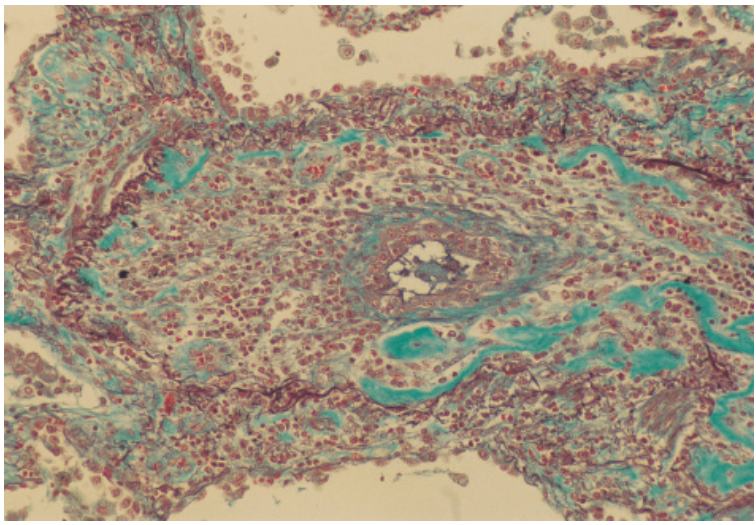

Fig. 4-30. Bronchiolitis obliterans in a florid state. A microphotograph of membranous bronchiole cross-sectioned, with the lumen strongly narrowed due to active inflammatory changes extending in the subepithelial layer. Elastica-Goldner stain.

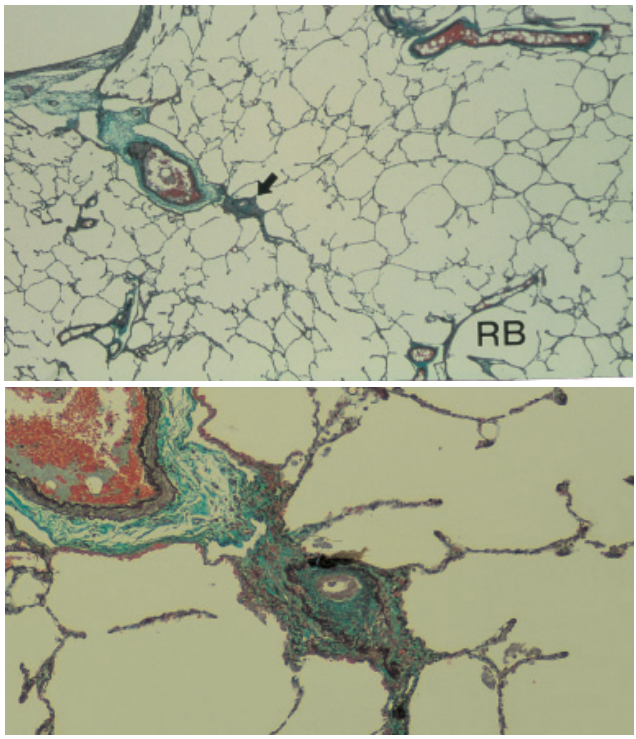

Fig. 4-31. Bronchiolitis obliterans in another case (scarring phase). Upper: a membranous bronchiole attenuated due to dense fibrosis, with the lumen left only as a pinhole (arrow). RB: respiratory bronchiole. Lower: the obstructed bronchiole magnified. Elastica-Goldner stain.

d) Three-D mapping of airway obstruction in bronchiolitis obliterans

The airway change in bronchiolitis obliterans (Figs. 4-30, 4-31)

Shown in Fig. 4-30 is the change of membranous bronchiole found in the lung of a patient having rheumatoid arthritis and dying of severe obstructive respiratory failure. The subepithelial layer is thickened with diffuse inflammatory changes, leaving only a pinhole lumen. This is a rare disorder called bronchiolitis obliterans (Seggev *et al.,* 1983) which is associated with either viral infection of affected bronchiole, rheumatoid arthritis or graft-vs. host disease, but there are many cases where etiology cannot be established.

Figure 4-31 is the lung from another patient dying of bronchiolitis obliterans, a female aged 64 years, in whom the etiology was not clear. Closely watching the lung sections, only a few, strongly obstructed bronchioles were found as in the figure. Without signs of active inflammation, they were considered to be in the state of postinflammatory scarring. Because such obstructed bronchioles were found only rarely in the sections, one may wonder whether the change can really have been responsible for developing respiratory distress that had been severe and apparently of obstructive nature. To obtain perspective about the state of the airway bed, a small scale reconstruction of the lung was undertaken by Yaegashi and Takahashi (1994).

Three-D mapping of bronchiolitis in the airway tree (Fig. 4-32)

Figure 4-32 exhibits a 3-D image of bronchioles in the lung shown in Fig. 4-31. The reproduced space measures 89 × 13 mm in the area of section and with a thickness of 3.1 mm. Now, the narrowing of airway bed, though ambiguous in routine microscopic examination, is clearly visible in this 3-D mapping. Obstructions, shown in

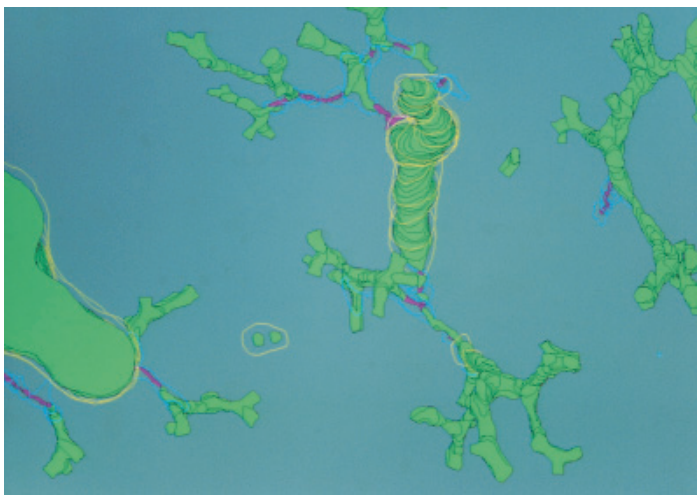

Fig. 4-32. Computer-assisted 3-D mapping of obstruction in a bronchiolar tree, in the lung shown in Fig. 4-31. Obstructions (purple) are exclusively involving the terminal bronchioles. More than 70% of the airway bed is obstructed. Reproduced from Yaegashi and Takahashi (1994): Arch Pathol Lab Med 118, pp. 979.

Fig. 4-33. Adenoma (A) and an early adenocarcinoma (C) of large intestine. The adenoma is connected with the intestinal mucosa with a slender stalk. Operation was performed to remove the carcinoma, with the adenoma coincidentally detected.

purple, are seen exclusively involving the terminal bronchioles; more than 70% of them are obstructed, but it is only a short segment of terminal bronchioles, 0.3 to 1 mm, that has been involved. One may understand in this situation why the lesions were not easily detectable in routine sections, causing the observers to underestimate the seriousness of disease. Thus, this may be a typical example showing that 3-D morphology works as an indispensable tool in revealing structure-function correlation.

e) Multistep carcinogenesis of the large intestine

Adenoma and adenocarcinoma of large intestine (Fig. 4-33)

It is now generally accepted that carcinoma of the large intestine arises, not directly from an ordinary mucosa, but usually from a sort of polyp that precedes. Polyp is a generic term expressing an elevated lesion arising in mucosa or skin. When examined endoscopically, subjects in the middle or advanced age are shown very often harboring polyps in their large intestine. Of the various sorts of intestinal polyps, those most common and prone to cancerous changes are the adenoma, which therefore is regarded as a precancer. Figure 4-33 demonstrates a segment of large intestine resected for an early carcinoma (C), but in the same material one can find another lesion, an adenoma having a slender stalk (A).

Vogelstein's hypothesis (Fig. 4-34)

In terms of microscopic features, carcinomas arising in the large intestine are mostly adenocarcinomas. This means that the carcinoma cells, having originated from

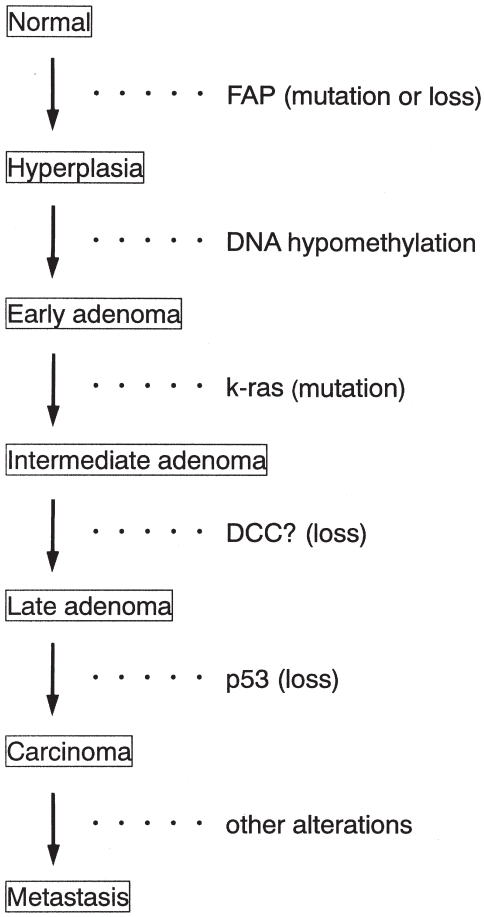

Fig. 4-34. Vogelstein's hypothesis proposed to explain the molecular background for multistep development of adenocarcinoma from adenoma of the large intestine.

the glandular epithelia of mucosa, continue to express more or less signs of differentiation as secreting cells. In the case of large intestine, carcinogenesis is considered to start with transformation of normal epithelia into hyperplastic cells. In the next place they are subjected to change into adenoma cells with mild cellular abnormalities, next into those with moderate and then into those with severe abnormalities, and then finally into overt carcinoma cells. Vogelstein *et al.* (1988) assume that each of these steps may be associated with a change of DNA (Fig. 4-34), meaning that the whole process of carcinoma development is a summation of molecular changes, or what is today spoken of as the multistep carcinogenesis. It seems likely therefore that each of the intermediate changes, such as adenoma with varying grades of cellular abnormalities, is a microscopic expression corresponding to a certain step in the assumed series of DNA changes.

Various grades of atypia in colonic tumors (Fig. 4-35)

Today, as growing number of adenomas are excised at endoscopic examination of large bowel, pathologists have come to experience tumors with various grades of cellular abnormalities. Such abnormalities are expressed as cellular atypia (see Chapter 8), and it is meant with this term that the higher the grade of atypia, the more does the malignant potential increase. Thus the disease ranges from adenoma with mild epithelial atypia to moderate to severe atypia and to overt carcinoma. Not infrequently, a single tumor is found consisting of zones with different grades of atypia, as observed in a 2-D microscopic section where zones of different atypia appear as patches that neighbor one upon another in mosaic fashion. Therefore if a tumor comprising areas with different atypia is submitted to 3-D mapping by reconstruction, the distribution of such areas may be visualized, allowing one to see their extension and mutual relation. Also, one can judge from the reconstructed image of the cut end whether or not a part of tumor is left unexcised.

In Japan, cellular atypia in these tumors is graded into five steps as in Fig. 4-35 (Japanese Society for Cancer of the Colon and Rectum, 1997). In this grading system, Group 1 means normal epithelial cells, Group 2 epithelial cells with mild atypia, Group 3 those with moderate and Group 4 with severe atypia. Group 5 denotes overt carcinoma. In Western countries, adenocarcinoma of large bowel is defined based on whether or not the tumor has started to grow invasively. This is different from the definition

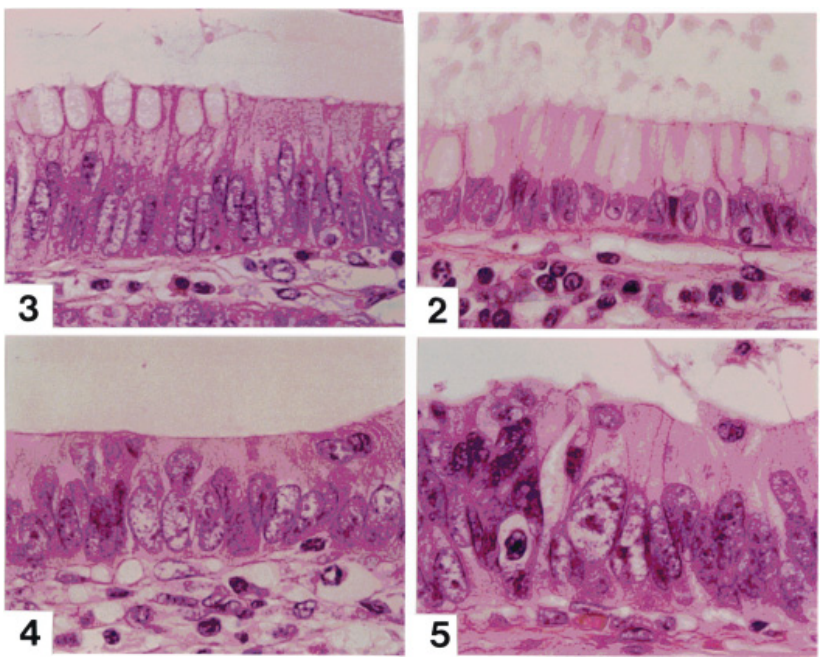

Fig. 4-35. Various grades of cellular atypia found in tumors of the large intestine ranging from adenoma with mild atypia (Group 2), that with moderate (Group 3) and severe atypia (Group 4), and overt adenocarcinoma (Group 5). Hematoxylin-eosin stain.

commonly used in Japan, where a carcinoma, even when remaining in the mucosa, is defined as such if the cells look sufficiently atypical and there are structural abnormalities such as the back-to-back pattern without intervening stroma. The latter feature and its significance will be discussed in the next chapter. In this study we conformed to these Japanese criteria.

Three-D reconstruction of adenoma harboring carcinoma (Fig. 4-36)

As many as 50 adenomas taken endoscopically were submitted to computer-assisted 3-D mapping of atypical areas by Zhang *et al*. (1994). An example of mapping is shown in Fig. 4-36 which is from a large adenoma, about 1.4 cm in largest diameter. The mass was sequentially sectioned at a comparatively large interval of 200 μm. This is because the study was designed so as to deal with such a large number of cases. It was preferred therefore to obtain an approximate knowledge about the distribution of atypia rather than to achieve the highest technical precision.

In this figure, there are patches of mild atypia (Group 2, yellowish green) which however are found as small fragmental remains after being replaced by moderate atypia (Group 3, faintly pink). The latter is shown to have extended almost over the whole surface, but within this, small areas with severe atypia have arisen (Group 4, dark pink), and in one of these, overt carcinoma is shown developing (Group 5, red).

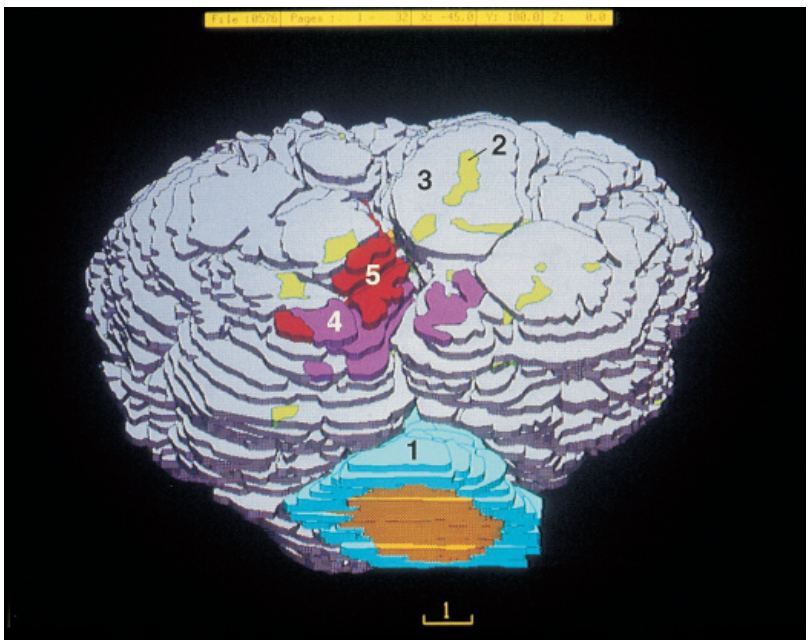

Fig. 4-36. Computer-assisted 3-D reconstruction of colonic polyp harboring lesions with various grades of atypia. Note that in adenoma with moderate atypia (Group 3, pink), adenoma with severe atypia (Group 4, dark pink) has developed, and in the latter, overt adenocarcinoma (Group 5, red) is arising, thus presenting a concentric zonation of increasingly malignant lesions. Reproduced from Zhang, Takahashi, *et al*. (1994): Pathology and Clinical Medicine 12, pp. 1397.

Thus, the distribution of atypia is clearly multizonal. Roughly speaking, different zones are arranged in a concentric fashion, with carcinoma at the center, which is surrounded by Group 4, which is then by Group 3 and so forth. Quite possibly, this distribution seems to be reflecting the multistep carcinogenesis as its morphological expression.

Distribution of carcinoma in 17 adenomas (Fig. 4-37)

In the tumor reconstructed in Fig. 4-36, the stalk is shown having normal epithelia (Group 1, green), making us confirm that neither adenoma nor carcinoma has attained at the stump. Of the 50 adenomas examined, 17 proved to harbor carcinoma in the form of "cancer in adenoma," all of which are arranged in Fig. 4-37 to show the distribution of carcinoma. The values entered in the figure are the percentile share of carcinoma in the whole mucosal volume contained in the polyps. In five of these, carcinoma was shown infiltrating into the submucosal layer, as indicated by an arrowhead. In one of them, carcinoma was shown extending so far as to reach the stump, requiring an additional surgery. In this case (Case 40), carcinoma at the stump would have been hard to detect without performing serial sections analysis.

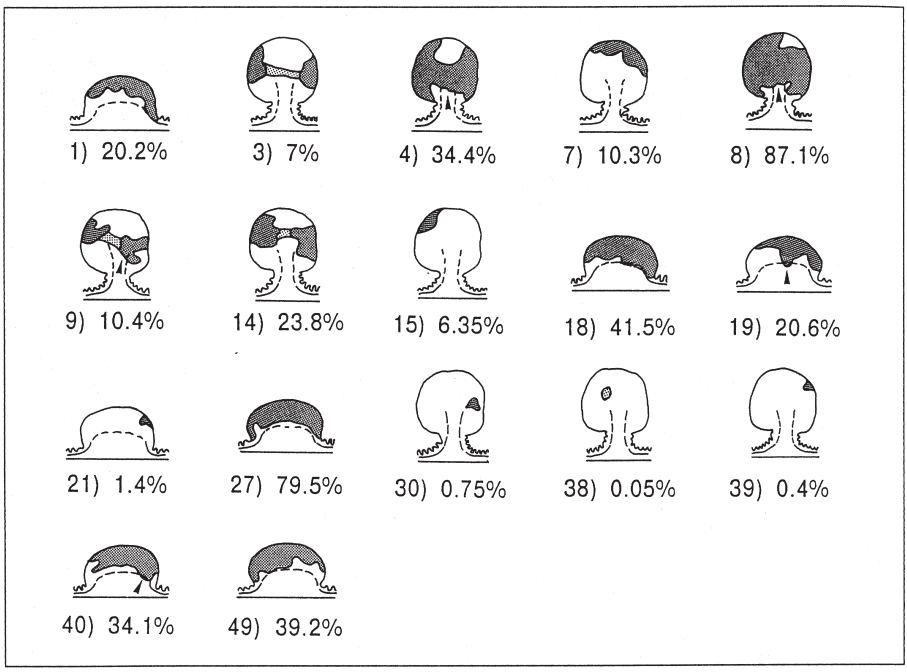

Fig. 4-37. Distribution of carcinoma schematically presented in 17 of the 50 adenomas reconstructed. The values entered are the percentile share of carcinoma in the whole mucosal volume contained in the polyps. In Case 40, carcinoma was shown reaching the stump. Reproduced from Zhang, Takahashi, *et al*. (1994): Pathology and Clinical Medicine 12, pp. 1399.

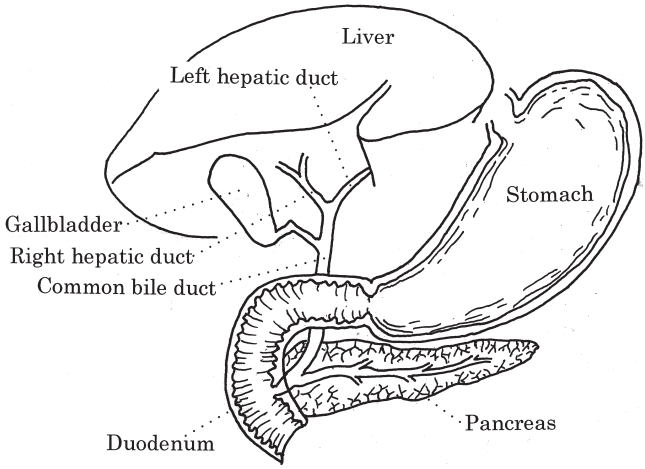

Fig. 4-38. A schema showing the anatomy of hepatohilar bile ducts.

f) The development and extension of hepatohilar bile duct carcinoma

Hepatohilar bile ducts (Fig. 4-38)

The extrahepatic part of bile ducts includes the right and left hepatic ducts, the cystic duct, the common bile duct and the duodenal papilla (see Fig. 4-38). Carcinoma often arises in this domain and is called hepatohilar bile duct carcinoma.

Cholangiogram of patient having hepatohilar bile duct carcinoma (Fig. 4-39)

Figure 4-39 is a cholangiogram of the patient having carcinoma developing from the common bile duct. In this patient, a catheter had been inserted through the abdominal wall into a dilated intrahepatic bile duct in order to drain away the accumulated bile, and the roentgenogram was taken after contrast medium was instilled through the catheter. Clearly, the intrahepatic ducts are strongly dilated due to bile stasis. This is the result of obstruction with carcinoma growing in the common bile duct, where the ductal lumen is shown abruptly coming to an end (arrow). In this situation, it is possible that carcinoma cells are not confined to the place of ductal obstruction; probably they have already extended along the ductal mucosa replacing the surface epithelial cells in the form of carcinoma in situ (CIS). However, about the extension of CIS-type carcinoma along the intra-and extrahepatic bile ducts, no reliable information is provided by any means available, including the X-ray imaging shown in the present figure. Thus, it still remains difficult for surgeons to establish an effective, pathology-based strategy against this tumor, and because of this, the tumor belongs to one of the most intractable cancers (Langer *et al*., 1985). In an effort to provide knowledge about the way this tumor develops and extends in the biliary tree in strict histopathological terms, Suzuki *et al*. (1989, 1998) attempted at 3-D mapping of carcinoma and precarcinomatous lesions (dysplasia) in the hepatohilar and intrahepatic biliary tree.

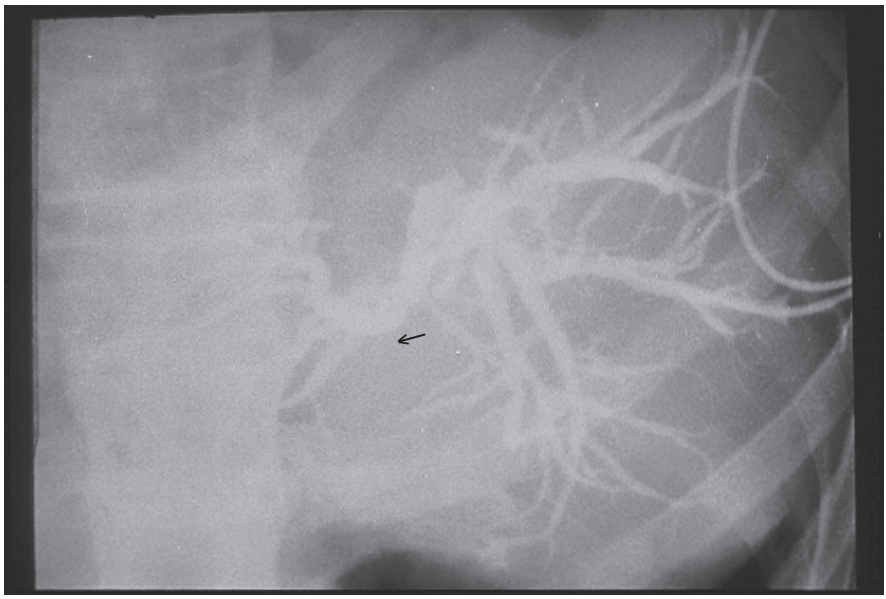

Fig. 4-39. A cholangiogram taken in a patient having hepatohilar bile duct carcinoma. Note the strongly dilated intrahepatic biliary tree. The tree is severed at the trunk, the common bile duct (arrow), showing a complete obstruction due to growth of carcinoma.

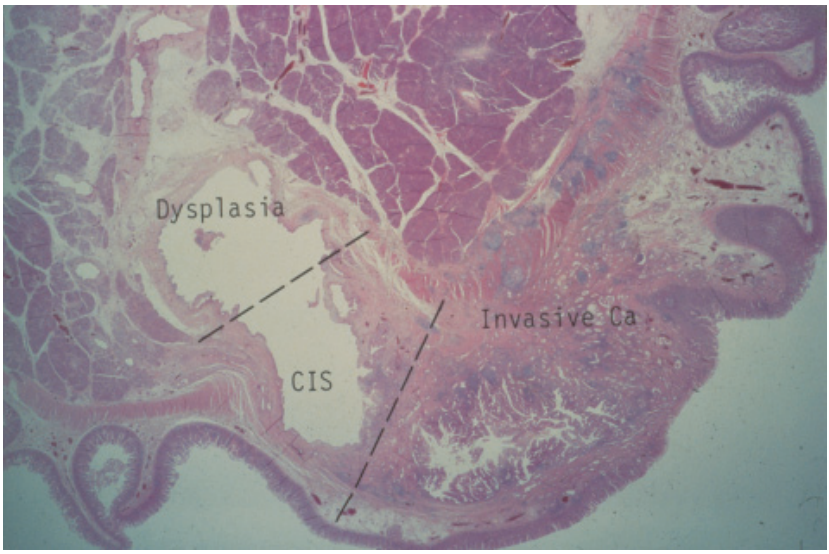

Fig. 4-40. Carcinoma of common bile duct developing at the lowermost portion (ampulla). A low power microphotograph. Carcinoma is invading around the duct and beneath the duodenal mucosa, but in the upper part, carcinoma extends non-invasively as CIS (carcinoma in situ) along the mucosal surface. In the more upper part, precarcinomatous cells (dysplasia) are extending, reaching the upper surgical margin. Hematoxylin-eosin stain.

Invasive carcinoma, CIS and dysplasia: distribution (Fig. 4-40)

Figure 4-40 is a low-magnified microphotograph of carcinoma arising at the lowermost portion of the common bile duct. The tumor is infiltrating around the duct and beneath the duodenal mucosa, but in the neighboring upper part, CIS (carcinoma in situ) is extending along the mucosal surface replacing the epithelia but without invading the subepithelial tissues. In the more upper part, there is an area of dysplasia where the surface epithelia of mucosa is replaced by atypical cells which however are not abnormal enough for giving a diagnosis of carcinoma. The term dysplasia is used to express the latter sort of change, and generally connotes that the atypical cells are in a precarcinomatous state. Thus, an invasive carcinoma is likely to be surrounded by a zone of CIS, which then is surrounded by another zone of dysplasia, and here again, we may expect a multistep carcinogenesis expressed in the form of concentric zonation.

Various grades of dysplasia in superficial mucosal cells (Fig. 4-41)

While microscopically examining bile ducts in materials taken from patients of hepatohilar bile duct carcinoma, one may find various grades of atypia distributed in a

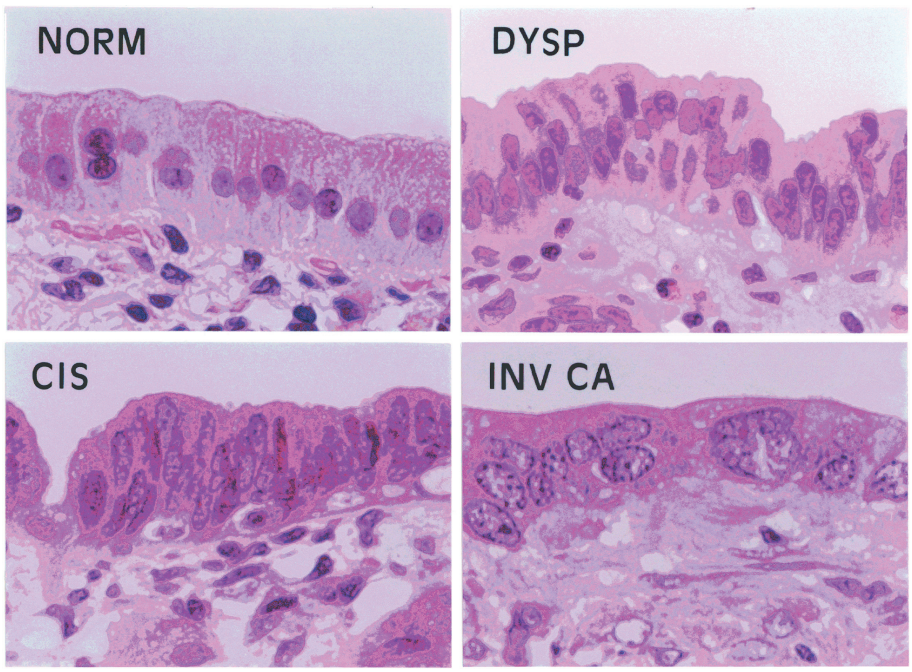

Fig. 4-41. Various grades of atypical cells found in bile duct. Normal (NORM), dysplasia (DYSP), carcinoma in situ (CIS) and invasive carcinoma (INV CA).

mosaic. Some examples are shown in Fig. 4-41 which includes normal bile duct epithelia, dysplastic cells, carcinoma in situ (CIS) and invasive carcinoma. One can confirm the cellular atypia advancing in this order.

Whole liver reconstruction from "macroserials" (Figs. 4-42, 4-43)

In many cases, surgical treatment of hepatohilar bile duct carcinoma includes resection of hepatohilar bile ducts involved in carcinoma, together with the part of the liver into which CIS-type carcinoma is assumed to be extending along the intrahepatic bile ducts. Therefore in performing 3-D reconstruction of biliary tree, a partially excised liver has to be subjected to serial slicing, where the thickness of a single section is required to be as thin as 1 mm. Serial slicing of this voluminous and flabby organ at a uniform thickness of 1 mm, if manually attempted, is next to impossible. After several trials, we found it workable to use a ham slicer, a simple device widely used in processing edible meat (Suzuki *et al*., 1988). The method ensures to obtain a serial 1-mm slices from a formalin-fixed liver lobe. The slices were "embedded" in gelatin to "fix" the flabby hepatoduodenal ligament containing the common bile duct. Figure 4-42 displays an example of liver thus sliced sequentially into what we call "macroserials."

Figure 4-43 exhibits a 3-D reconstruction of the intrahepatic biliary tree in a whole liver which was obtained at autopsy and had carcinoma in the gallbladder. The organ was sliced into as many as 223 serial slices to visualize the distribution of carcinoma. The figure however was designed so as to show only the anatomy of normal bile ducts, not distinguishing among the normal, dysplastic and carcinomatous segments.

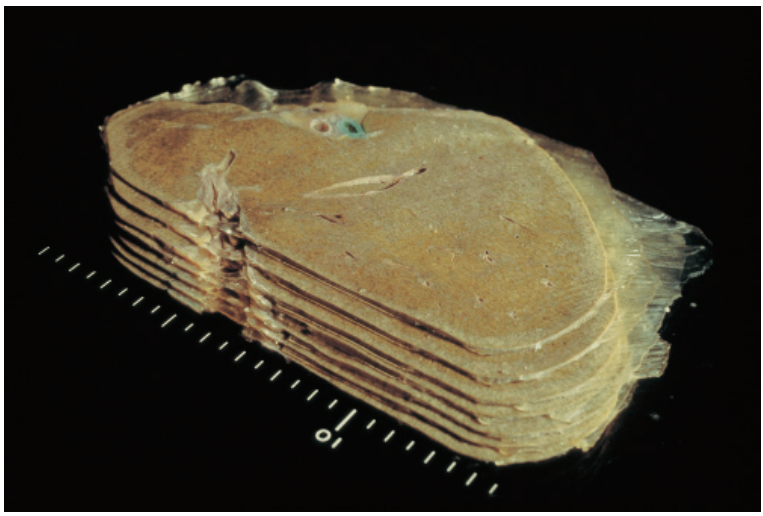

Fig. 4-42. Preparation of "macroserials," serial slicing of surgically excised liver lobe, gelatin embedded, into 1mm-thick slices using a ham slicer. Also see page 97-98. Reproduced from Suzuki, Takahashi *et al*. (1989): Cancer 64, pp. 660.

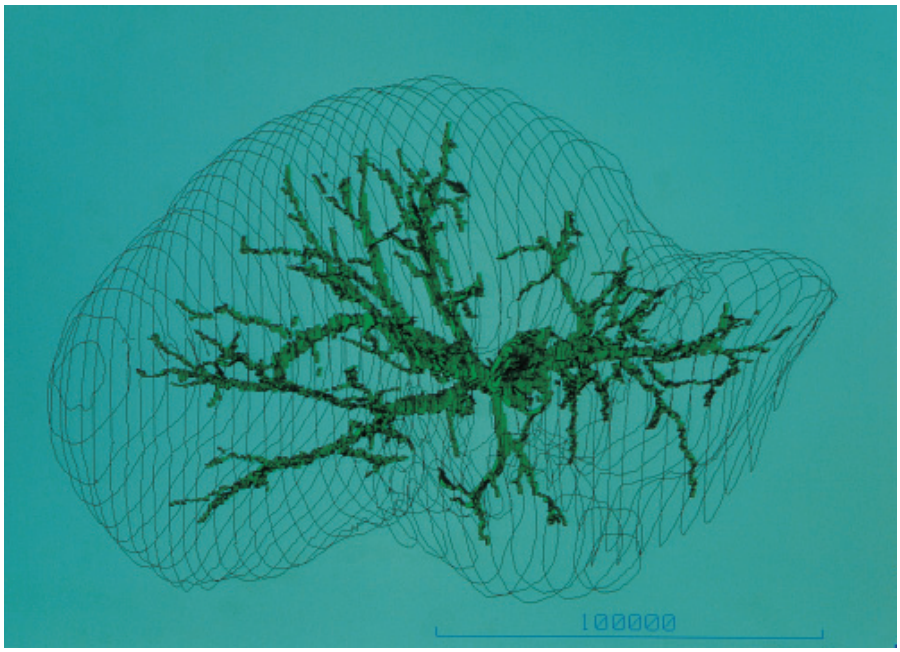

Fig. 4-43. Computer-assisted 3-D reconstruction of a whole liver taken at autopsy to show the intrahepatic biliary tree. The liver was sliced into 236 "macroserials." A case of gallbladder carcinoma.

Three-D mapping of carcinoma in the biliary tree (Fig. 4-44)

An example of 3-D mapping is shown in Fig. 4-44. This is from a patient in whom the left liver lobe was resected for carcinoma arising from the left hepatic duct. Painted green are ducts lined with normal epithelia. Carcinoma is shown growing in the left hepatic duct that is painted in red, where partially the tumor is infiltrating periductally, as indicated by yellow wireframes. There are segments painted blue, and these indicate ducts lined by dysplastic epithelia. It is clearly visualized that 3-dimensionally, the ducts with epithelial dysplasia are so arranged as to surround the duct having carcinoma. Thus the pattern of distribution seems to be suggesting that a zone of dysplasia had been extending before carcinoma developed within the zone, and once again we find an expression of multizonal advancement of malignant transformation. Carcinoma, not reaching the stump at either the right hepatic or common bile duct, seems to have totally been removed. However, dysplasia has already extended down to these stumps, leaving the possibility that ducts having this precancerous lesion remain unexcised in the patient, awaiting future malignant changes.

The 3-D mapping was extended so as to include as many as 26 patients operated for hepatohilar bile duct carcinoma (Suzuki *et al*., 1999). Out of the 26 livers, as many as 21 (81%) proved to have a dysplastic zone around carcinoma. Thus, hepatohilar bile duct carcinoma arising from dysplasia seems to be quite common.

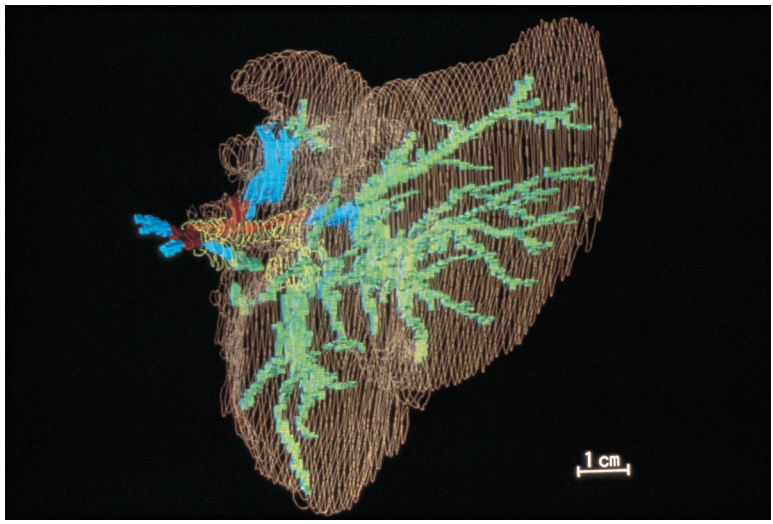

Fig. 4-44. Computer-assisted 3-D mapping of tumors in the biliary tree of the left liver lobe resected for carcinoma arising in the left hepatic duct. Bile duct segments having carcinoma are painted in red, those with dysplasia in blue and normal ducts in green. Note that carcinoma is surrounded by segments having dysplasia, demonstrating a sort of concentric zonal arrangement and suggesting that the carcinoma has arisen in a pre-existing zone of dysplasia. Reproduced from Suzuki, Takahashi, *et al*. (1989): Cancer 64, pp. 662.

g) Intraductal papilloma of breast: extension and cancer development

A breast comprises several lobes (Fig. 4-45)

A unilateral human breast contains 15 to 20 glandular lobes, each drained by a segmental (lactiferous) duct which opens at the lactiferous sinus just below the nipple. Toward the periphery, the duct divides many times, forming a tree of mammary ducts. In the schema of Fig. 4-45, a breast is illustrated so as to contain four lobes.

Intraductal papilloma: microscopic appearance (Fig. 4-46)

Sometimes, papillary tumor arises from the epithelia lining the mammary ducts and extends intraductally forming a ductal cast as schematically shown in the foregoing figure. This tumor is called intraductal papilloma and appears on microscopic section as multiple tumors (Fig. 4-46). Not infrequently, carcinoma arises in intraductal papilloma, but the accurate site of ductal tree where carcinoma develops had not been known. Also, we cannot determine on a 2-D section whether there is a single dividing tumor or there are multiple tumors, since the tumor extends in the finely arborizing ductal tunnels. In Fig. 4-45, the right schema illustrates an intraductal tumor which is single and united, while in the left, there are multiple tumors. However, we cannot determine which of the two possibilities is the case, so long as our observation is confined to a sectional picture, for example, that of the plane along the broken line. In this situation, it requires 3-D visualization of ductal tree to obtain information about the development and extension of intraductal papilloma and its relation to carcinoma. This was performed by Ohuchi *et al*. (1984a) who studied breast lobes excised from 15 patients with intraductal papilloma.

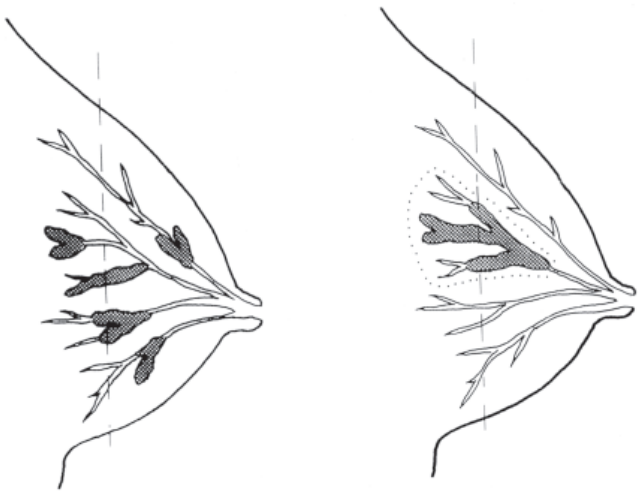

Fig. 4-45. Ducts and lobules of breast: a schema. Carcinomas as well as pre-carcinomatous lesions of the breast develop in the tree of mammary duct, but whether the ductal system harbors a single tumor or multiple tumors cannot be determined by observing a section shown by the broken line. In both the left and right pictures, three sections of tumor appear in the cutting plane.

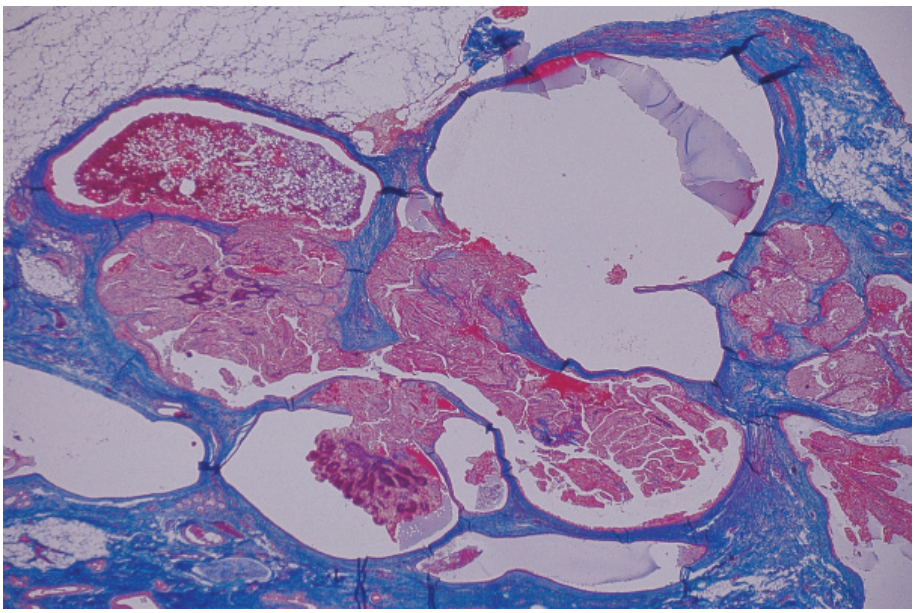

Fig. 4-46. Intraductal papilloma of the breast: a low power microphotograph. There are tumors growing in several ducts, but their connecting relation in the ducts is not visible on a single 2-D section. Azan-Mallory stain.

Three-D mapping of intraductal papilloma (Figs. 4-47, 4-48)

Figure 4-47 is a semi-schematic presentation of reconstructed ducts in a patient with papilloma. The material was a single mammary lobe taken by segmentectomy. Smaller subbranches having no tumor are omitted from the figure for the sake of better perspective. In the figure, one can find a total of nine papillomas, each extending in

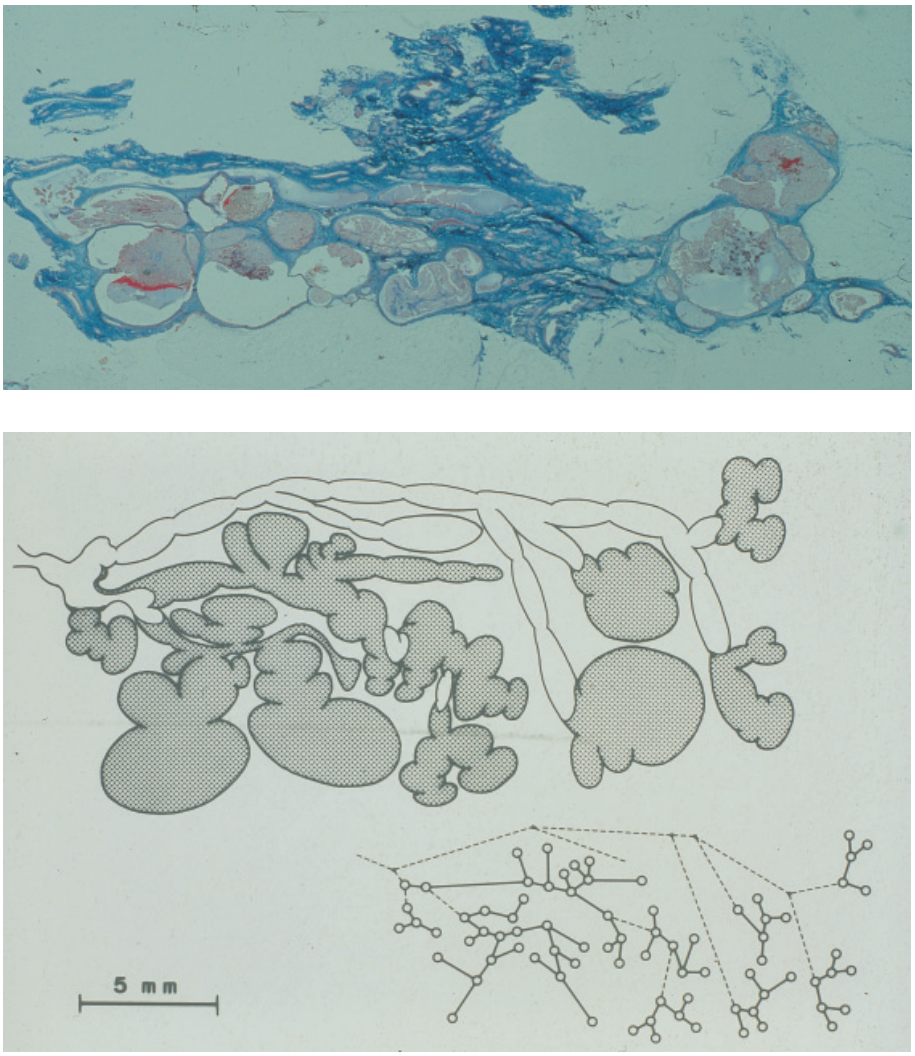

Fig. 4-47. Manually performed 3-D mapping of intraductal papillomas in the ductal tree of one mammary lobe. A half-schematized presentation. As a whole there are nine tumors, each rooted at a terminal segment of the ductal tree, suggesting that all the tumors have developed from the terminal segments. Reproduced from Ohuchi, Takahashi *et al*. (1984): Breast Cancer Res Treat 4, pp. 122.

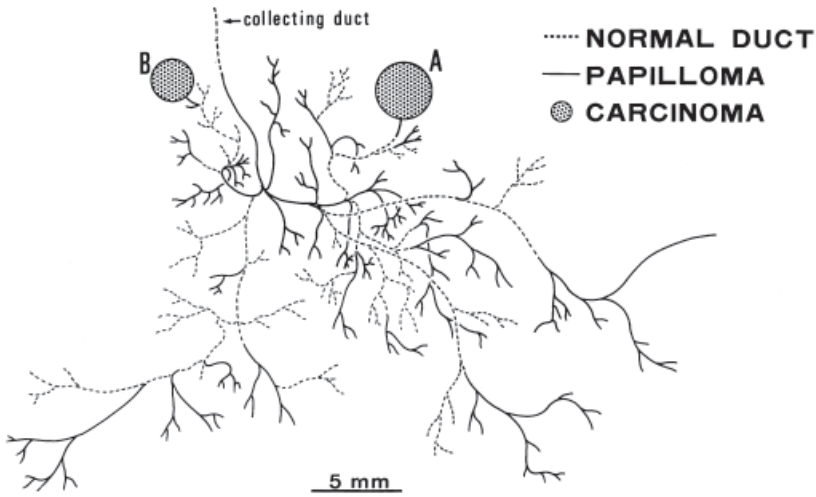

Fig. 4-48. Manual 3-D mapping of intraductal papillomas, another case. Here, a mammary lobe proved to contain a total of 18 papillomas (solid line), all of which are rooted at the treetop. The broken lines are ducts having no tumor. At two places, denoted with A and B, minute carcinoma was detected to be arising in papilloma. Reproduced from Ohuchi *et al*.(1984): Cancer 54, pp. 610.

the branching ducts but independent of the others. It is worthy of attention that without exception, all the nine papillomas are rooted somewhere at the terminal ending of the ductal tree. This seems quite likely to be suggesting that this type of papilloma arises in the terminal segment of mammary ducts, usually as multiple tumors and growing intraductally toward the nipple.

Figure 4-48 is another 3-D mapping of ducts from another patient of intraductal papilloma performed by Ohuchi *et al*. (1984b), again in the form of schematic presentation. Here too, the arborizing ducts contained in a lobe are reproduced, where the broken lines denote the segments having normal epithelia and the solid lines, those harboring papilloma. One can confirm that the ductal tree contains a total of 18 independent papillomas, and here again, all of the tumors have a root at the ductal terminal. In this case, however, minute carcinoma was found developing at two places, as denoted with A and B.

Three-D mapping study of intraductal papilloma: summary (Fig. 4-49)

The results of 3-D mapping performed in a total of 15 cases of intraductal papilloma are summarized in Fig. 4-49. In all patients the material was a single mammary lobe surgically excised by segmentectomy. Comparison of the results led to the conclusion that from a 3-D distribution point of view, intraductal papillomas are classifiable into two types. In one, the tumor develops in a larger segment usually as a single mass. This type was found in five of the 15 cases, and in none of them carcinoma

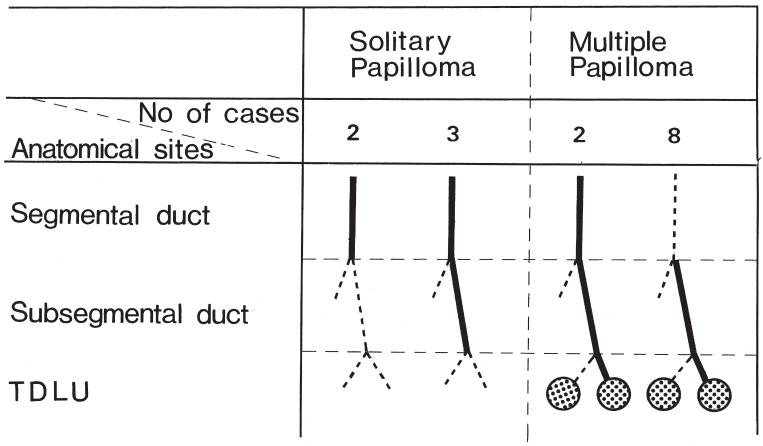

Fig. 4-49. A summary of 3-D mapping of papilloma in 15 patients. It turned out that the intraductal papillomas were classifiable into two types: multiple and solitary. The former arises in the terminal segments and can secondarily develop carcinoma, whereas the latter grows in the larger part of the ductal tree as a single mass, where no cancer development was demonstrated. Reproduced from Ohuchi, Takahashi *et al*. (1984): Breast Cancer Res Treat 4, pp. 126.

proved to be arising. The pattern of distribution was different in the remaining 10 patients; here the tumor presents as multiple masses developing from the treetop of the ductal system. Carcinoma, when found in papilloma, never failed to arise in the latter type.

h) Three-D microanatomy and pathology of human pancreas

Two types of ischemic necrosis: central and peripheral (Figs. 4-50, 4-51)

While microscopically examining autopsy material, ischemic necrosis of the pancreas is found, not infrequently. Such necroses occur when the blood flow of pancreas is severely impaired, for example in patients who have been in the state of cardiac insufficiency or shock. We noticed from a microstructural vewpoint that two types of necroses were discernible. In one, as in the microphotograph of Fig. 4-50, necrosis involves the islet of Langerhans. This type of necrosis involves the central area of "primary lobule," a unitary structure of the pancreas, which we defined as below. Therefore we designated this type as "central necrosis." Entered in the lower part of the figure is a manual 3-D reconstruction from this pancreas. There are two necrotic foci (hatched), each containing a large islet supplied by an afferent arteriole.

The other type is "peripheral necrosis." Here, as in Fig. 4-51, necrosis develops so as to surround an islet at a distance, while the islet itself remains exempted from ischemic injury. This type of necrosis is considered to extend along the peripheral zone of the "primary lobule." In the lower part of the figure, portions of two large (secondary) lobules are reconstructed. Shaded are the necrotic foci, mostly sitting on the interlobular septa. Note that the islets are uninvolved, kept apart from the lesions.

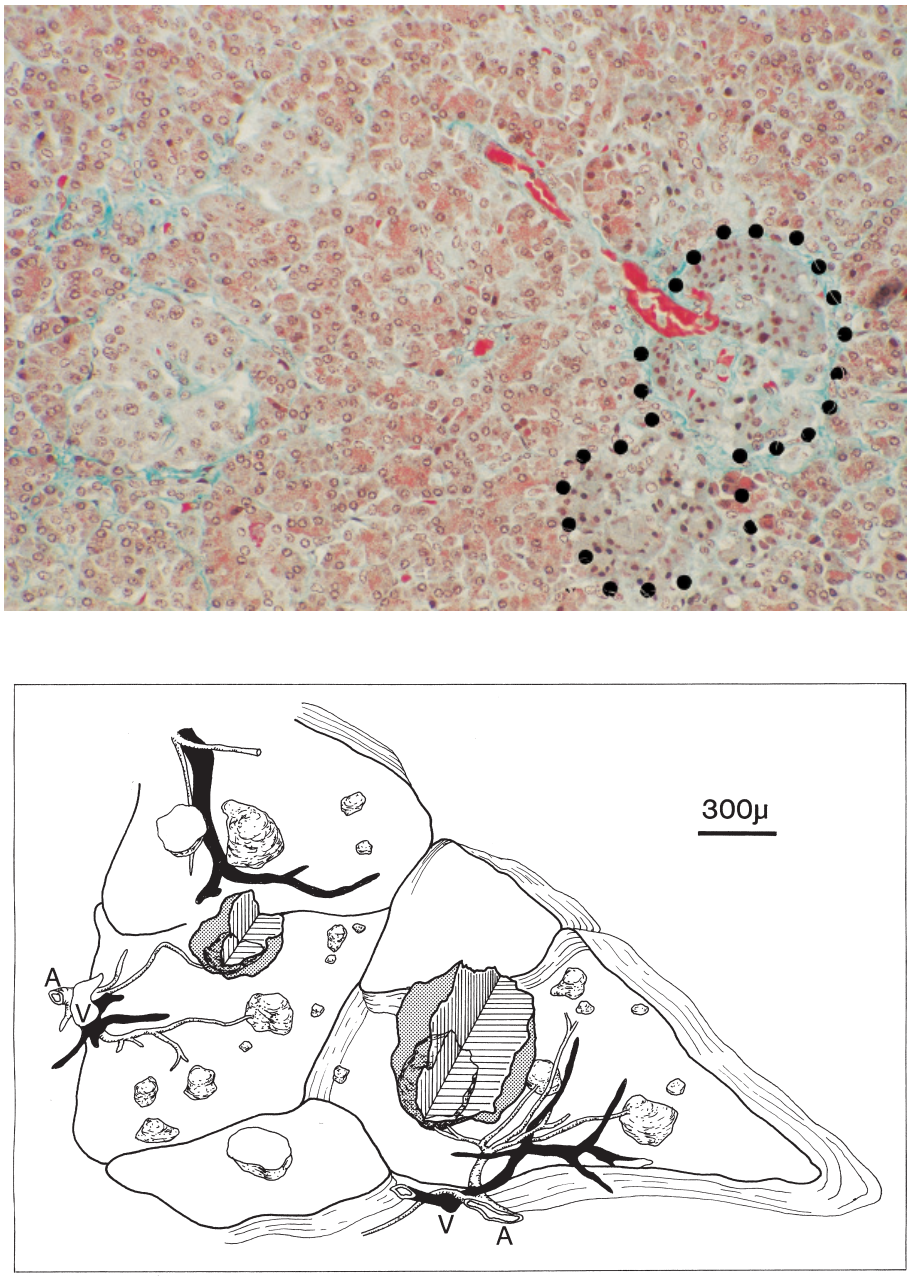

Fig. 4-50. The central type of ischemic pancreatic necrosis. (Upper) Necrosis involves two islets and surrounding excretory tissue (encircled by dots). Elastica-Goldner stain. (Lower) Manual reconstruction from a part of the pancreas containing five primary lobules. There are two necrotic foci (hatched), each having an islet. The lower figure reproduced from Takahashi, Yaginuma *et al*. (1985): Path Res Pract 179, pp. 647.

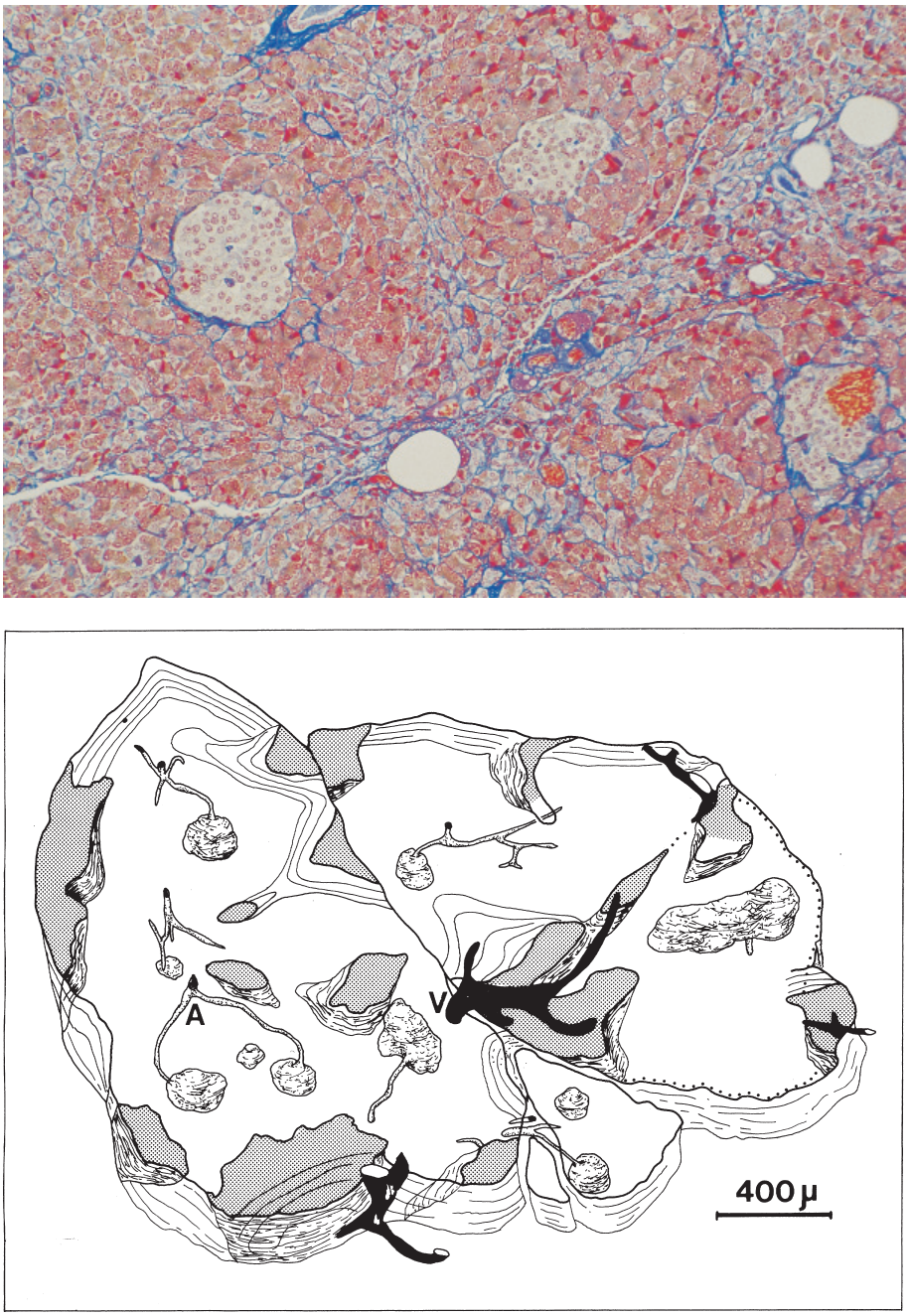

Fig. 4-51. The peripheral type of ischemic necrosis. (Upper) Necrotic belts are surrounding well-sustained areas, each having an islet at the center. Azan-Mallory stain. (Lower) Manual reconstruction showing the necrotic foci (hatched) distributed along venules (V) and surrounding the islets at a distance. A: arteriole. The lower figure reproduced from Takahashi, Yaginuma *et al*. (1985): Path Res Pract 179, pp. 649.

Three-D vasculature of the pancreas (Fig. 4-52)

Since the lesions are ischemic in origin, the difference in morphogenesis of the two types of necrosis may become clear if the basic microvasculature pattern of the human pancreas is established. However, what had been known of the pancreatic vasculature was limited to the intimate anatomical association of islets with arterioles, a finding described in the early 1930s by Beck and Berg (1931). In this view, Yaginuma *et al*. (1986) and Takahashi *et al*. (1985) performed manual 3-D reconstruction of pancreases taken at autopsy to see what pattern of vasculature exists, underlying the development of such ischemic lesions. Shown in Fig. 4-52 is the microvasculature of a normal pancreas reproduced from serial sections by manual method. Two lobules are included in the figure, each containing Langerhans' islets of various dimension. Pairs of interlobular artery (white) and vein (black) are shown running within the interlobular septum, entering the lobules and dividing in the lobular parenchyma.

Four different types of relationship proved to exist between the terminal arterioles and islets:

Type 1: Arteriole that terminates at a large islet and serves as its vas afferens
Type 2: Long arteriole that ends in the peripheral zone of lobule
Type 3: Arteriole having one or more small islets dispersed around its ending
Type 4: Arteriole stemming from interlobular artery, directly entering a lobule and ending at an islet

Despite the variety in the pattern of arterial ending, larger islets are supplied without exception by an afferent arteriole.

Fig. 4-52. Manually performed 3-D reconstruction of the pancreatic microvasculature. Two lobules are included. White: interlobular artery. Black: interlobular vein. Many islets are dispersed in the lobules. The relation of islets with terminal arteries is various, allowing to classify into four types, as denoted in the figure by 1, 2, 3 and 4. Reproduced from Yaginuma, Takahashi *et al*. (1986): Pathol Res Pract 181, pp. 80.

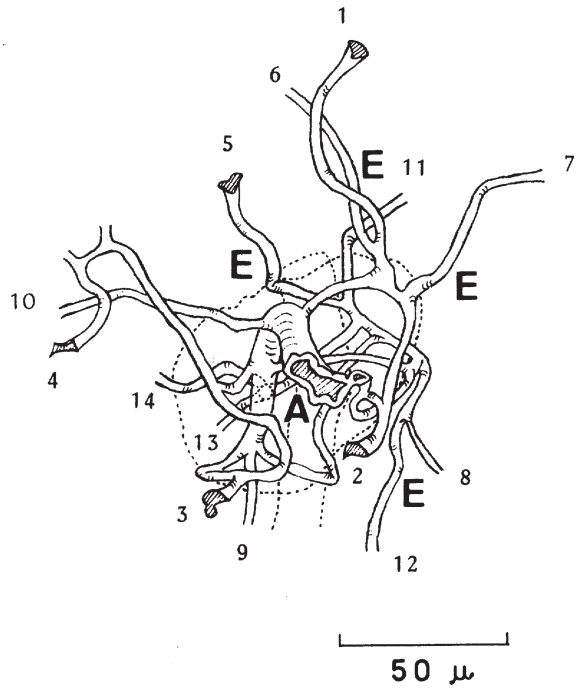

Fig. 4-53. Manual 3-D reconstruction of minute vessels in and around a medium-sized islet. An afferent arteriole (A) enters the islet and divides into a glomoid network of capillaries. A total of 14 efferent vessels (E) leave the islet and connect with the capillary network of the surrounding exocrine tissue. Reproduced from Yaginuma, Takahashi *et al*. (1986): Pathol Res Pract 181, pp. 81.

Vasculature of a Langerhans' islet (Fig. 4-53)

In Fig. 4-53, 3-D vasculature in and around an islet of Langerhans is visualized. An afferent arteriole (A) is shown entering the islet. It divides into a glomoid network of capillaries. Blood leaves the islet, in this figure through 14 efferent vessels (E), and irrigate the capillary network of the surrounding exocrine tissue so that the hormones secreted by the islet cells may be carried directly to the exocrine region.

Summary of pancreatic vasculature: the primary lobule (Fig. 4-54)

The basic pattern of pancreatic microvasculature was abstracted from Fig. 4-52 and summarised in Fig. 4-54. The schema illustrates that the lobule of the pancreas is an assembly of smaller structural units, each having a terminal arteriole at the center and flanked by venules. We designated these units as the primary lobules of pancreas with a connotation that the conventional lobules wrapped by connective tissue septa are to be called the secondary lobules. Sometimes the central arteriole does not supply an Langerhans' islet directly, but the islets never fail to find themselves at the center of the primary lobule so that the exocrine tissue, surrounding an islet or islets, may always be irrigated by blood containing islet hormones just secreted. Between the arte-

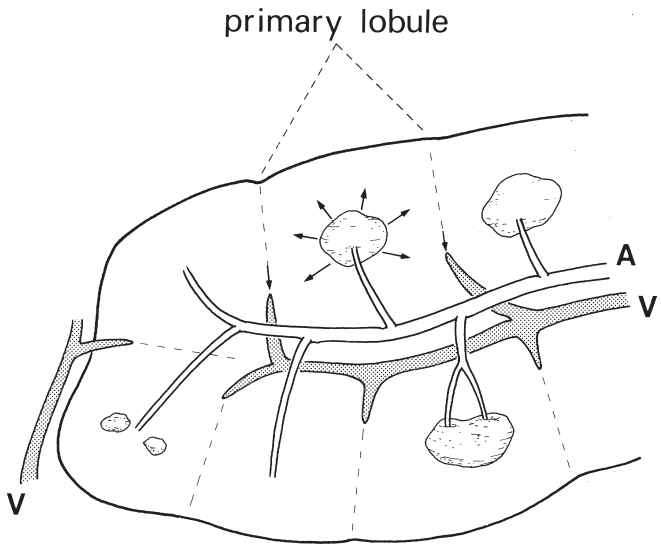

Fig. 4-54. The basic pattern of pancreatic microvasculature. A branch of terminal arteriole (A) is assigned to irrigate a small unitary area, which we call a primary lobule. A primary lobule has a terminal arteriole at the center and flanked by venules (V). Islets, whether or not directly supplied by an afferent arteriole, are always positioned at or near the central portion of primary lobule. The conventional lobule surrounded by connective tissue septa (the secondary lobule) is an assembly of primary lobules. Reproduced from Takahashi, Yaginuma, *et al*. (1985): Pathol Res Pract 179, pp. 646.

rioles (A) and venules (V) one can find an alternating (interdigitating) relation, where a certain degree of isodistance seems to exist.

Two types of ischemic necrosis related with the microvasculature (Fig. 4-55)

Based upon the structural principle induced above, we are now able to explain the difference in pathogenesis of the two types of ischemic necrosis (Fig. 4-55). The development of "central necrosis," i. e., ischemic necrosis involving the central zone of primary lobule, may be understood if we assume that arterial blood flow is blocked at the most peripheral segment. Such a segment corresponds to the arteriole supplying a primary lobule; when the primary lobule has a larger islet, the arteriolar segment functions as its afferent arteriole. Upon this type of ischemia, the peripheral zone of primary lobule may be exempted from ischemia because collateral blood can flow in from the neighboring primary lobules. In contrast, "peripheral necrosis" is considered to occur when a more proximal arterial segment is severely but imperfectly obstructed. In this case, the obstructed arterial segment may be responsible for supplying an area of pancreas containing, for example, tens or hundreds of primary lobules. Then, for individual primary lobules, no collateral flow from the adjacent ones can be expected. Thus, it may be the periphery of primary lobules that is most vulnerable to deficient bloody supply, since the zone corresponds to the part remotest from the afferent arteriole through which blood flows in.

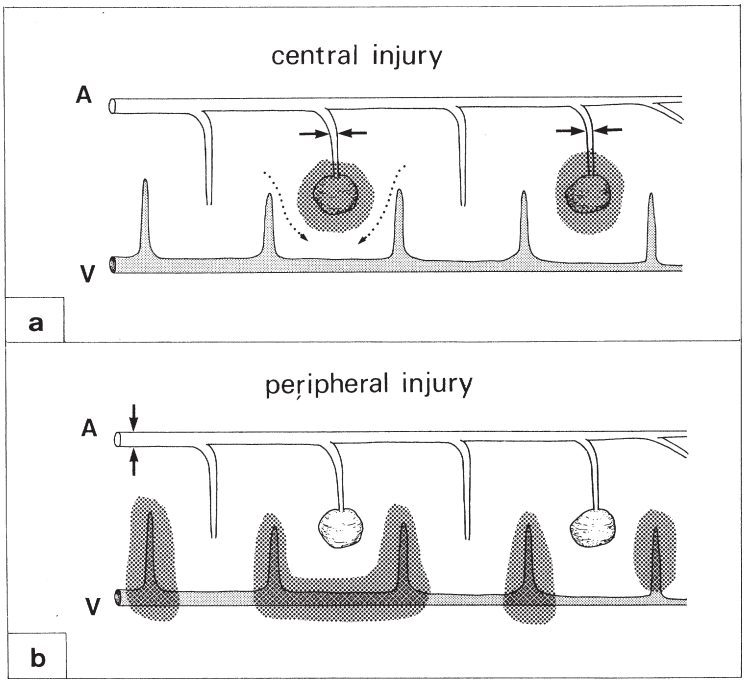

Fig. 4-55. The two types of ischemic necrosis is correlated with the microvasculature shown in Fig. 4-54. The central necrosis (a), involving the central portion of primary lobules, is explained by assuming that the blood flow is blocked at the terminal arteriole. Collateral blood flow, from the neighboring primary lobules, relieves the peripheral zone of primary lobules. In contrast, the peripheral necrosis (b) is understood by assuming an obstruction at a more proximal arterial segment. In this case, the periphery of primary lobules is the site most susceptible to ischemia. Reproduced from Takahashi, Yaginuma, *et al.* (1985): Pathol Res Pract 179, pp. 650.

The lobule of the pancreas and its anatomical significance (Fig. 4-56)

Also to be introduced are another series of pancreatic studies by Watanabe *et al.* (1997, 1999) who performed 3-D reconstructions of pancreas with computer assist. Figure 4-56 demonstrates an adult human pancreas which was analyzed to examine whether the "lobules," not primary but the secondary ones defined by the connective tissue septa, are a vascular or a ductal unit. Reconstruction disclosed that the demarcation of lobules by the membranes (black wireframes) was quite imperfect with many holes gaping in the septa, through which the parenchymal tissue proved to be continuing. Most lobules, however, were found to receive a single duct (yellow), justifying to define them as "glandular lobules." Exceptions to this rule were not rare because sometimes, lobules were found receiving not only a lobular duct of their own but a small accessory duct from the neighboring lobule. There was no finding giving support for assuming that the lobules are a vascular unit, because from any viewpoint, they were not corresponding to any territories of arterial supply or venous drainage.

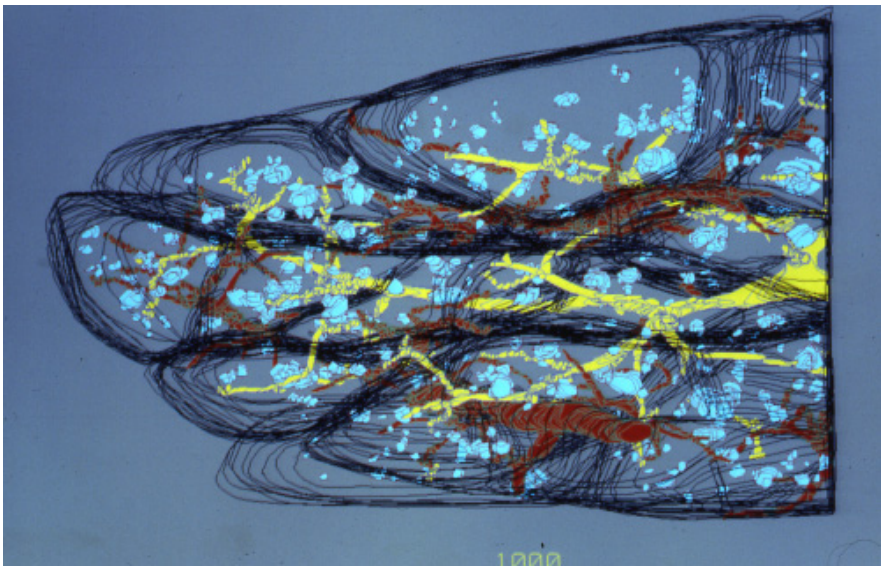

Fig. 4-56. Computer-assisted 3-D reconstruction of normal pancreas to understand the anatomical significance of the (secondary) lobules. Note that the demarcation with the septa (black wireframes) is imperfect and penetrated by large holes, through which the parenchymal tissue and ducts (yellow) continue. However, most lobules are shown receiving a single duct, justifying to define them as glandular units. Reproduced from Watanabe, Takahashi, *et al*. (1997): Pancreas 15, pp. 50.

Islet-duct relation: changes with the development (Figs. 4-57, 4-58, 4-59)

It is well known that in the human, pancreatic islets arise in an early period of gestation from the primitive pancreatic ducts as insular buds (Like *et al*., 1972). Thereafter the islets are supposed to separate from the ducts and disperse throughout the lobules, but little has been known about how they migrate to take the ultimate spatial distribution in the lobule. To visualize the developmental process of pancreas in this context, its microstructure was studied by computer-assisted 3-D reconstruction.

Specimens of fresh autopsy pancreases from three fetuses, three neonates and three adults were submitted to serial sectioning and 3-D reconstruction of one secondary lobule. Representative pictures from each of the three age groups are exhibited in Figs. 4-57, 58 and 59, respectively. In the pancreas of a fetus, 24 gestational weeks (Fig. 4-57), small number of islets (light blue) were found, all of them still remaining in direct contact with the ducts (yellow). In a neonate on the first postnatal day (Fig. 4-58), 31 islets were contained in the lobule; 23 of these were still retaining contact with ducts, whereas the other eight (violet) were separated from the ducts and going to disperse in the exocrine tissue. In the pancreas of an adult, 47-year-old male (Fig. 4-59), 52 of the 101 islets in the reconstructed lobule were still having contact with ducts, while the others had migrated far into the peripheral lobular zone. This transition of islets from the periductal to more peripheral zone seemed to ensure direct effects of islet hormones on the exocrine part of the pancreas. However, even in adults,

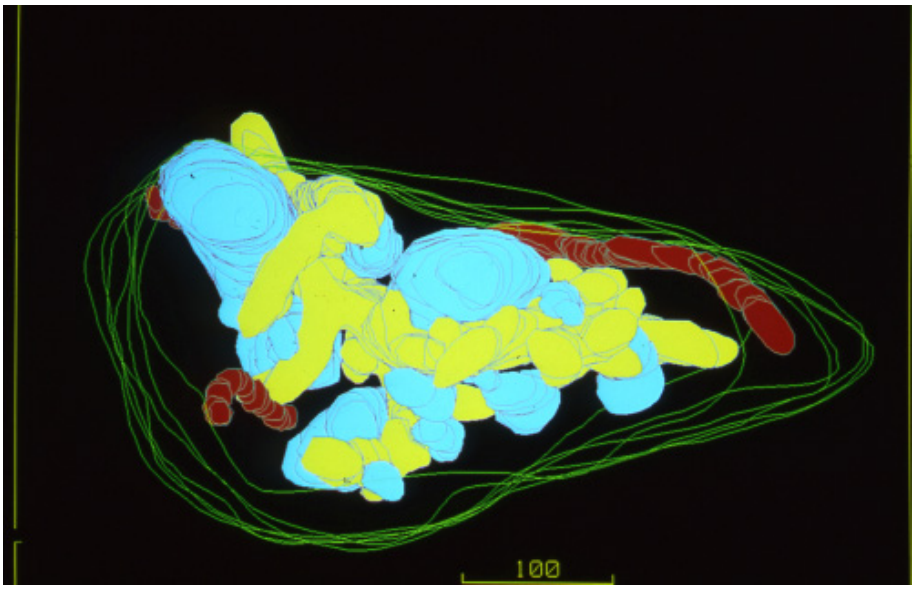

Fig. 4-57. Computer-assisted 3-D reconstruction of a fetal pancreas, 24 gestational weeks. In this stage of development, all the islets (light blue) remain as buds sprouting from the ducts (yellow). Arteries are painted in red. Reproduced from Watanabe, Takahashi, *et al*. (1999): Pancreas 18, pp. 351.

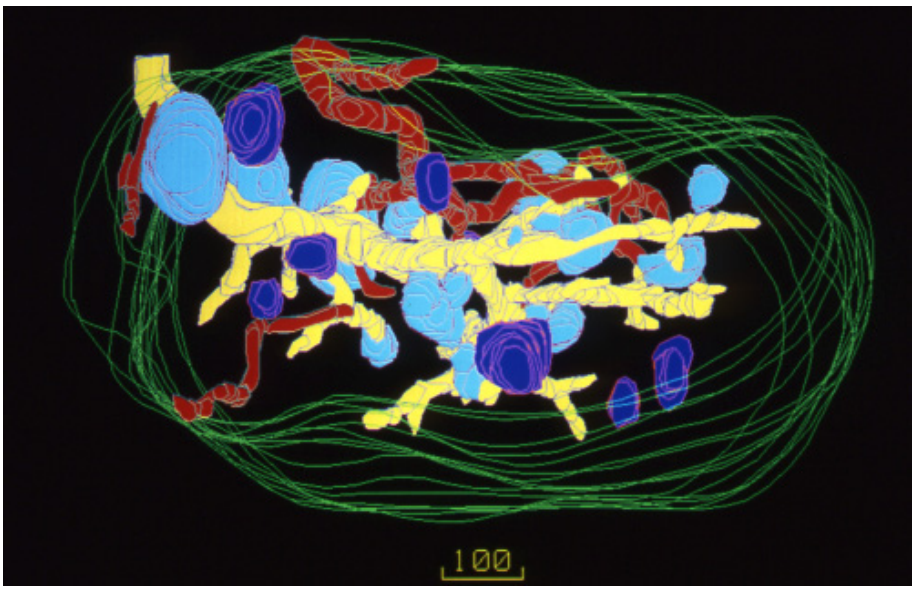

Fig. 4-58. Computer-assisted 3-D reconstruction of a neonatal pancreas. Most of the islets (light blue) are still retaining connectivity with the ducts, but there are small number of islets (violet) that have left the ducts and dispersed into the exocrine region. Reproduced from Watanabe, Takahashi, *et al*. (1999): Pancreas 18, pp. 351.

as many as half of the islets in a lobule were shown remaining next to the ducts. It seems possible that the latter group of islets are spare parts that will be mobilized in case of need, for example when a majority of peripheral islets have been destroyed. About this possibility, however, further studies have yet to be done.

i) The microanatomy of terminal liver vessels and bile ducts (Figs. 4-60, 4-61)

One of the serious complication of liver transplantation is the so-called vanishing bile duct syndrome, a progressive loss of intrahepatic bile ducts observed in chronically rejected allografts. Though much remains unknown about the causative factors of duct loss, the development of vascular lesions, particularly of hepatic arteries, seems playing an important role (Oguma *et al*., 1989). However, little is known in the first place about the normal vascular supply of small intrahepatic bile ducts *of man*. In view of this, Takemura *et al*. (1991) undertook 3-D reconstruction of small bile ducts, peripheral hepatic arteries and portal veins in small portal tracts of normal livers and failed allografts, in order to visualize the basic pattern of vascular supply and to correlate the level of arterial obstruction with ischemic changes of ducts. As in Figs. 4-60 and 4-61, it was shown that in normal livers, interlobular bile ducts were wrapped by a dense peribiliary capillary network. Of the peripheral branches of hepatic arteries, some were confirmed running parallel with ducts, from which, branches were divided and sent to the network. We designated the former as the "accompanying arteries," and the latter as "communicating arteries." There were also arteries running indepen-

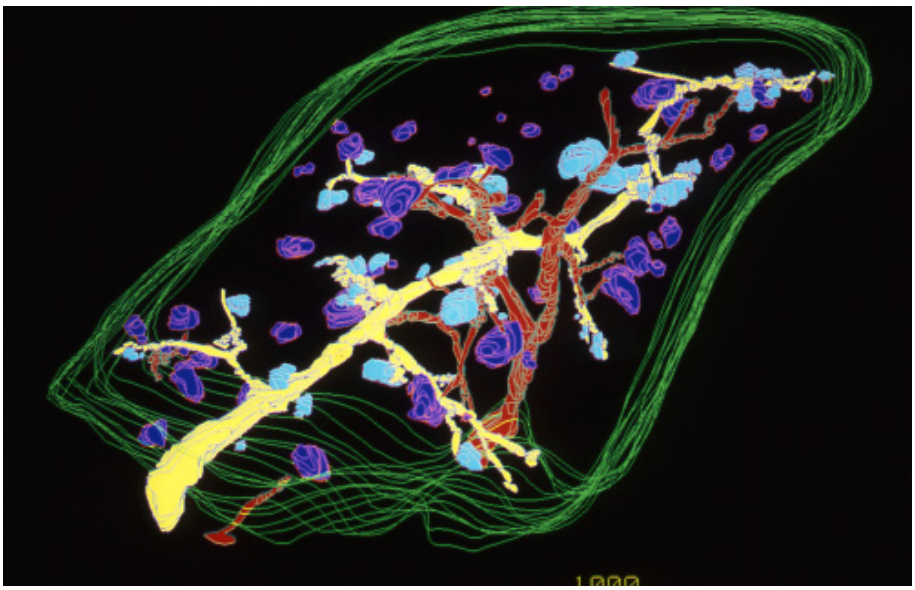

Fig. 4-59. Computer-assisted 3-D reconstruction of an adult pancreas. About half the islets have left the ducts and migrated far into the peripheral zone of lobule. Reproduced from Watanabe, Takahashi, *et al*. (1999): Pancreas 18, pp. 351.

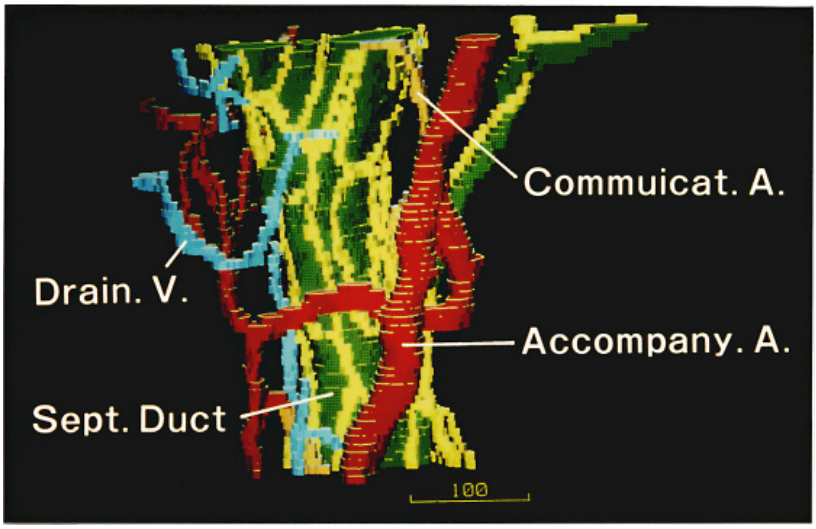

Fig. 4-60. Computer-assisted 3-D reconstruction of a peripheral bile duct and blood vessels in its surroundings, in a normal human liver. An interlobular duct (green) is wrapped by a dense peribiliary capillary network (yellow). There is a small artery running in parallel with the duct (the accompanying artery), from which small branches (communicating arteries) are divided and sent to the peribiliary network. Also, there is an artery running independently of the duct and directly pouring blood to the sinusoid. The peribiliary network is drained by a small portal vein (light blue). Reproduced from Takemura, Takahashi *et al*. (1991): Transplant Proc 23: 1410.

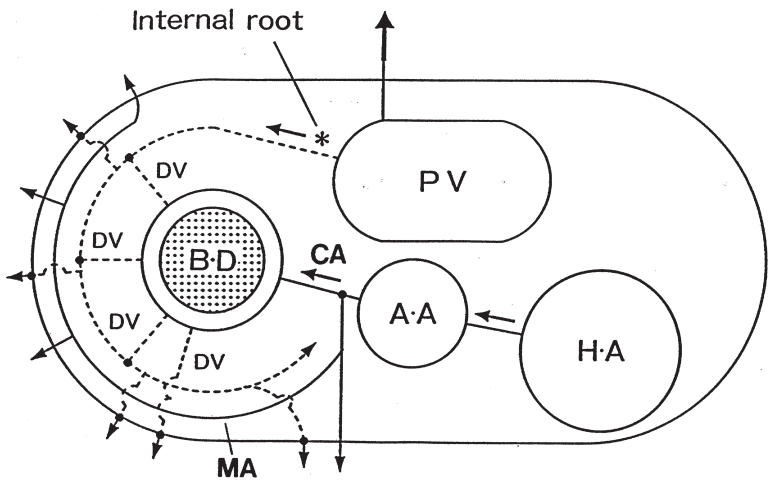

Fig. 4-61. A schema illustrating the microanatomy of peripheral bile duct (BD), its blood supply and drainage. HA: large hepatic artery, AA: accompanying artery, CA: communicating arteriole, PV: potal vein, DV: draining venule. Reproduced from Takemura, Takahashi, *et al*. (1991): Transplant Proc 23, 1409 – 1412.

dently of ducts and leading directly to the intralobular sinusoids. The network is drained by a small portal vein running at a distance, which is connected with the peribiliary network with "internal roots." This is the basic pattern of peribiliary vasculature, which probably was the first demonstration for the liver *of man*, since previous knowledge had been either more or less fragmental or obtained from the liver of rodents. In the failed allografts severe arteriopathy proved to exist, where arteries were obstructed with proliferating intimal cells containing foam cells. Such changes were shown involving various levels of small arteries, including the accompanying and communicating arteries. Areas of network corresponding to obstruction were severely destroyed with significantly reduced density of capillaries.